Green-function theory of confined plasmons in coaxial cylindrical geometries: Finite magnetic field

M. S. Kushwaha[1,2] and B. Djafari-Rouhani[2]

[1]*Institute of Industrial Science, University of Tokyo, 4-6-1 Komaba, Meguro-Ku, Tokyo 153-8505, Japan*
[2]*UFR de Physique, CNRS 8024, University of Science and Technology of Lille I, 59655 Villeneuve d'Ascq Cedex, France*
(Received 27 July 2004; revised manuscript received 22 November 2004; published 19 May 2005)

We report on a theoretical investigation of plasmon propagation in the coaxial cylindrical geometries using Green-function (or response-function) theory in the presence of an applied axial magnetic field ($\vec{B} \| \hat{z}$). The magnetoplasmon excitations in such multiple-interface structures are characterized by the electromagnetic (EM) fields that are localized at and decay exponentially away from the interfaces. Green-function theory, when generalized to be applicable to such quasi-one-dimensional systems, enables us to derive explicit expressions for the corresponding response functions (associated with EM fields), which can in turn be used to compute numerous physical properties of the system under consideration. A rigorous analytical diagnosis of the general results in diverse situations leads us to reproduce exactly the previously well-established results on planar systems, both in the presence and absence of $\vec{B}$, obtained within the different theoretical frameworks. As an application, we present several illustrative examples on the dispersion characteristics of the confined and extended magnetoplasmons in the single- and double-interface structures. These dispersive modes are also substantiated through the computation of local as well as total density of states. It is found that, unlike as in the zero-field case, the magnetoplasma propagation is nonreciprocal with respect to the sign of the index m of the Bessel functions involved. The effects of an applied magnetic field and the aspect ratio on the dispersion of the confined magnetoplasmons are discussed. We also briefly clarify some delusive traces of the edge magnetoplasmons for a plasma shell embedded between two identical or unidentical dielectrics. The elegance of theory lies in the fact that it does not require matching of the messsy boundary conditions and it also lies in its simplicity and the compact form of the desired results. Our theoretical framework can also serve as a powerful technique for studying the intrasubband plasmons and magnetoplasmons in the emerging mutiple-walled carbon nanotubes.

I. INTRODUCTION

Ever since the discovery of quantum Hall effects, semiconducting systems of reduced dimensions and size have been among the most important subjects of research in condensed matter physics. We refer specifically to the quasi-two-dimensional (Q2D), quasi-one-dimensional (Q1D) and quasi-zero-dimensional (Q0D) systems and their periodic counterparts, which are now known for providing a better understanding of how the charge carriers behave when confined to still lower dimensions. The tremendous research interest focused on these systems worldwide is reasonably attributed to advancements in thin-film growth and nanofabrication techniques that are allowing the synthesis of almost flawless heterointerfaces. A recent extensive review of the subject, both theoretical and experimental, can be found in Ref. 1.

The role of an applied magnetic field to probe the treasure of conventional solids has been appreciated long before the advent of the nonconventional solids.[2] This is because the effect of the magnetic field on the band structure is more striking and is easily observed in the experiments. A number of interesting phenomena originate from the alteration in the band structure due to the magnetic field, such as the Bloch states[3] yielding metallic conductivity,[3] the Landau diamagnetism,[4] the Shubnikov-de Haas effect,[5] the de Haas-van Alphen effect,[6] cyclotron resonance,[7] the appealing Hof-

stadter butterfly spectrum,[8] and 2D extended states below the localized Fermi energy responsible for the quantum Hall effect,[9] to name a few. These were investigated, and then serve as the diagnostic tools for characterizing the materials. A recent proposal where the resulting magnetization is shown to be a complementary tool for probing the shape of the quantum dots, for example, is quite encouraging.[10]

The ongoing advancements in nanofabrication technology lead us to imagine the formation of even more sophisticated structures such as quantum disks, pipes, snakes, balls, rings, and ribbons where electrons are confined in the regions with quasidimensionality between three-dimensional (3D) and zero-dimensional (0D) (see, for example, Ref. 1). The fabrication of essentially arbitrary geometries is expected to lead to dramatic control of the physical properties of solids. The role of the boundaries in understanding several electronic, optical, and transport phenomena in such nanostructures has been much appreciated in the recent past. We refer, in particular, to the importance of the edge states in understanding, for example, the magnetotransport in quantum Hall regimes in a broad range of mesoscopic systems.[1]

In this context, Pepper and co-workers[11] reported results on the band structure and conductance of axially symmetric, curved, noninteracting 2D electron gas (2DEG), topologically equivalent to a Corbino disk, in the presence of a non-homogeneous magnetic field, arising as the result of an applied axial magnetic field. They relied on the fact that the

development of regrowth technology, using *in situ* cleaning techniques, now allows one to investigate the effects of varying the topography of an electron gas in addition to varying its dimensionality. This offers the possibility of investigating the electron dynamics in a nonhomogeneous magnetic field, even though the originally applied magnetic field is homogeneous.

Despite the enviable advances in revealing and explaining the exotic behavior of nanostructures based on the emerging, sophisticated quantal theories, the optical phenomena being investigated within classical electrodynamics continue to receive considerable attention, especially the nanoscale cylindrical as well as the spherical structures. The cylindrical structures have generated particular interest for their usefulness, not just as electromagnetic waveguides, but also as atom guides, where the guiding mechanism is governed mainly by excited cavity modes. It is envisioned that the understanding of atom guides at such a small scale would lead to many desirable advancements in atom lithography, which in turn should facilitate atomic physics research.[12]

In this paper, we investigate, in general, the plasma modes of a semiconductor (dielectric) shell embedded between two unidentical dielectrics (semiconductors) in the coaxial cylindrical geometries using Green-function theory in the presence of an applied axial magnetic field. Our theoretical approach is virtually the interface response theory (IRT)[13] generalized to be applicable to quasi-one-dimensional (Q1D) systems subjected to an applied magnetic field. Ever since its inception, the IRT has been extensively applied to study various quasiparticle excitations (such as phonons, plasmons, magnons, etc.) in heterostructures and superlattices.[14–16] In the recent past, it was successfully extended to investigate collective excitations in diverse two-dimensional (2D) systems, both with and without applied magnetic fields.[17,18] Quite recently, we have studied the plasma modes in the coaxial cylindrical geometries in the absence of an applied magnetic field.[19] The present work is, in fact, a generalization of the work presented in Ref. 19 to include the axial magnetic field. Note that the electromagnetic modes in a single dielectric or metallic cylinder had been known for many years.[20]

The general results on the confined (or, nonradiative) as well as extended (or, radiative) magnetoplasmon dispersion, in both single-and double-interface geometries, are shown to be correctly substantiated by the computed local and/or total density of states. In addition, we have also performed a careful analytical diagnosis of the final general expressions to reproduce the well-established results, obtained within the different theoretical frameworks, on several planar geometries, both with and without an applied magnetic fields. Apart from such tests of the theory, we believe that it should prove to be a simple but powerful scheme of a theoretical framework for studying, for example, the intrasubband plasmons and magnetoplasmons in the multiwalled carbon nanotubes where theoretical research is gaining considerable momentum recently.[21]

This paper is organized as follows. In Sec. II, we discuss some basic notions of cylindrical geometry and calculate the bulk response functions in the presence of an applied axial magnetic field. In Sec. III, we present the theoretical formal-

ism for the inverse response functions to derive the final expressions for the magnetoplasmon dispersion relations, discuss an interesting analytical diagnosis of the general expressions under special limits, and give an explicit analytical relationship between the response functions and the density of states. In Sec. IV, we report several illustrative examples of numerical results on the magnetoplasmon dispersion and of the local and total density of states in a variety of experimentally realizable situations. Finally, in Sec. V, we conclude our findings and list some interesting dimensions worth adding to the problem in the future.

II. BASIC NOTIONS AND BULK RESPONSE FUNCTIONS

First, we consider that it is important to make a careful analysis of Maxwell's equations before using them in deriving the response functions for the respective systems. We consider the electromagnetic waves propagating with an angular frequency ω and wave vector $k \| \hat{z}$ in a medium defined by the cylindrical coordinates (ρ, θ, z). For the sake of generality, we consider every medium to be a semiconducting plasma, and the system is subjected to an applied axial magnetic field ($\vec{B} \| \hat{z}$). This implicitly means that we are, in a sense, working with the Faraday geometry (for details of the magnetic-field configurations, see Ref. 1). The plasma waves, here as well as in the latter part of this work, will be assumed to observe spatial localization along the direction perpendicular to the axis of the cylinder. It is also noteworthy that we are interested in the nonmagnetic materials, and this means that $\vec{B} \equiv \vec{H}$ in Maxwell's curl-field equations. The physical system is also assumed to be isotropic, albeit the presence of the magnetic field imposes an anisotropy in the system. The latter implies that in the Cartesian coordinates, for example, $\epsilon_{xx} = \epsilon_{yy}$, $\epsilon_{xy} = -\epsilon_{yx}$, and $\epsilon_{zx} = \epsilon_{xz} = \epsilon_{zy} = \epsilon_{yz} = 0$, and the longitudinal component ϵ_{zz} is, naturally, independent of the magnetic field (see Appendix A). For the sake of brevity, we will be working with $\epsilon_1 = \epsilon_{xx}$, $\epsilon_2 = \epsilon_{xy}$, and $\epsilon_3 = \epsilon_{zz}$.

To start with, we eliminate the magnetic-field variable $\vec{B}$ from Maxwell's curl-field equations to write

$$\vec{\nabla} \times (\vec{\nabla} \times \vec{E}) - q_0^2 \tilde{\boldsymbol{\epsilon}} \cdot \vec{E} = 0. \qquad (2.1)$$

Here the dielectric constant $\tilde{\epsilon}$ is a tensor quantity, since the system we are concerned with is subjected to an external magnetic field. In Eq. (2.1), $q_0 = \omega/c$ is the vacuum wave vector, where c is the speed of light in the vacuum. Note that in the presence of an applied magnetic field, Eq. (2.1) is the standard wave-field equation one starts with. We will use the convention that the EM fields obey the spatial and temporal dependence of the form of $\vec{A}(\rho, \phi, z) = \vec{A}(\rho)e^{(im\theta + ikz - i\omega t)}$, where $\vec{A} \equiv \vec{E}$ or $\vec{B}$. Recalling the standard definitions of $\vec{\nabla} \cdot \vec{A}$, $\nabla^2 \phi$ (with ϕ as any scalar), and $\vec{\nabla} \times \vec{A}$ in the cylindrical coordinates, we split the original Maxwell's curl-field equations in the cylindrical coordinates and evaluate the field components E_x, E_y, B_x, and B_y in terms of E_z and B_z, since we choose to work in terms of the latter components. The result, after straightforward manipulation, is

$$E_x = \frac{1}{\rho \alpha_1^4} \left\{ \left[iq_0^2 \epsilon_2 \rho \frac{\partial}{\partial \rho} B_z + m k_1^2 B_z \right] q_0 \right.$$
$$\left. + \left[-ik_1^2 \rho \frac{\partial}{\partial \rho} E_z + m q_0^2 \epsilon_2 E_z \right] k \right\}, \qquad (2.2)$$

$$E_y = \frac{1}{\rho \alpha_1^4} \left\{ \left[ik_1^2 \rho \frac{\partial}{\partial \rho} B_z - m q_0^2 \epsilon_2 B_z \right] q_0 \right.$$
$$\left. + \left[iq_0^2 \epsilon_2 \rho \frac{\partial}{\partial \rho} E_z + m k_1^2 E_z \right] k \right\}, \qquad (2.3)$$

$$B_x = \frac{1}{\rho \alpha_1^4} \left\{ \left[-ik^2 \epsilon_2 \rho \frac{\partial}{\partial \rho} E_z - m \alpha_2^2 \epsilon_1 E_z \right] q_0 \right.$$
$$\left. + \left[-ik_1^2 \rho \frac{\partial}{\partial \rho} B_z + m q_0^2 \epsilon_2 B_z \right] k \right\}, \qquad (2.4)$$

$$B_y = \frac{1}{\rho \alpha_1^4} \left\{ \left[-i\alpha_2^2 \epsilon_1 \rho \frac{\partial}{\partial \rho} E_z + m k^2 \epsilon_2 E_z \right] q_0 \right.$$
$$\left. + \left[iq_0^2 \epsilon_2 \rho \frac{\partial}{\partial \rho} B_z + m k_1^2 B_z \right] k \right\}, \qquad (2.5)$$

where $k_1^2 = (k^2 - q_0^2 \epsilon_1)$, $\alpha_1^4 = k_1^4 + q_0^4 \epsilon_2^2$, and $\alpha_2^2 = k_1^2 - q_0^2 \epsilon_2^2 / \epsilon_1$. Before we proceed further, we define the tenet of the interface response theory (IRT), the black-box surface (BBS). By the BBS we mean an entirely opaque surface through which electromagnetic fields cannot propagate. The idea of introducing the BBS in the IRT was conceived with two prominent advantages over the contemporary semiclassical approaches in mind. First, it allows one to disconnect entirely from the extra mathematical world, and hence to confine oneself only within the true building block of the system concerned. Second, it implicitly provides a great opportunity to get rid of using the messy boundary conditions one is so routinely accustomed to in dealing with inhomogeneous systems. In order to create a medium bounded by a black-box surface, we assume that Eqs. (2.2)–(2.5) are valid for either $\rho < R$ or $\rho > R$, with R as the radius of the only cylinder in question for now. In other words, we multiply the right-hand sides of Eqs. (2.2)–(2.5) by the step function $\theta(\rho - R)$ or $\theta(R - \rho)$, as the case may be. Evidently, the step function (and hence the Dirac-delta function) dictates the kind of physical situation we will need to consider in what follows. Then the z components of Maxwell's curl-field equations satisfied by $E_z(\rho, \theta)$ and $B_z(\rho, \theta)$ assume, after careful mathematical manipulation, the following forms:

$$\left(\frac{-iq_0 \alpha_2^2 \epsilon_1}{\alpha_1^4} \right) \left\{ \left[\frac{1}{\rho} \frac{\partial}{\partial \rho} \left(\rho \frac{\partial}{\partial \rho} \right) + \left(-\frac{\epsilon_3 \alpha_1^4}{\epsilon_1 \alpha_2^2} - \frac{m^2}{\rho^2} \right) \right] E_z - \left(\frac{kq_0 \epsilon_2}{\epsilon_1 \alpha_2^2} \right) \right.$$
$$\times \left[\frac{1}{\rho} \frac{\partial}{\partial \rho} \left(\rho \frac{\partial}{\partial \rho} \right) - \frac{m^2}{\rho^2} \right] B_z - \delta(R - \rho) \left[\frac{\partial}{\partial \rho} E_z + \left(\frac{imk^2 \epsilon_2}{\rho \epsilon_1 \alpha_2^2} \right) \right.$$
$$\left. \left. \times E_z - \left(\frac{kq_0 \epsilon_2}{\epsilon_1 \alpha_2^2} \right) \frac{\partial}{\partial \rho} B_z + \left(\frac{imkk_1^2}{\rho q_0 \epsilon_1 \alpha_2^2} \right) B_z \right] \right\} = 0, \qquad (2.6)$$

and

$$\left(\frac{iq_0 k_1^2}{\alpha_1^4} \right) \left\{ \left[\frac{1}{\rho} \frac{\partial}{\partial \rho} \left(\rho \frac{\partial}{\partial \rho} \right) + \left(-\frac{\alpha_1^4}{k_1^2} - \frac{m^2}{\rho^2} \right) \right] B_z + \left(\frac{kq_0 \epsilon_2}{k_1^2} \right) \right.$$
$$\times \left[\frac{1}{\rho} \frac{\partial}{\partial \rho} \left(\rho \frac{\partial}{\partial \rho} \right) - \frac{m^2}{\rho^2} \right] E_z - \delta(R - \rho) \left[\frac{\partial}{\partial \rho} B_z + \left(\frac{imq_0^2 \epsilon_2}{\rho k_1^2} \right) \right.$$
$$\left. \left. \times B_z + \left(\frac{kq_0 \epsilon_2}{k_1^2} \right) \frac{\partial}{\partial \rho} E_z - \left(\frac{imk}{\rho q_0} \right) E_z \right] \right\} = 0. \qquad (2.7)$$

The coefficients of $\delta(R - \rho)$ in these equations stand for the perturbation(s) required for creating the black-box surface(s) needed in the formulation of the problem. The formal equations (2.6) and (2.7) will be the standard format for all the calculations of the Green-functions of the system of interest in what follows. For the sake of brevity, we will henceforth use the following notations:

$$\gamma_1^2 = q_0^2 \epsilon_1 - k^2 = -k_1^2$$
$$\gamma_2^2 = q_0^2 \epsilon_v - k^2 = -\alpha_2^2, \qquad (2.8)$$
$$\gamma_3^4 = \gamma_1^4 + q_0^4 \epsilon_2^2 = \alpha_1^4$$

where $\epsilon_v = (\epsilon_1 + \epsilon_2^2 / \epsilon_1)$. Then the unperturbed parts of Eqs. (2.6) and (2.7) assume the following forms:

$$\left(\frac{iq_0 \epsilon_1 \gamma_2^2}{\gamma_3^4} \right) \left\{ \left[\frac{1}{\rho} \frac{\partial}{\partial \rho} \left(\rho \frac{\partial}{\partial \rho} E_z \right) + \left(\frac{\epsilon_3 \gamma_3^4}{\epsilon_1 \gamma_2^2} - \frac{m^2}{\rho^2} \right) E_z \right] + \left(\frac{kq_0 \epsilon_2}{\epsilon_1 \gamma_2^2} \right) \right.$$
$$\left. \times \left[\frac{1}{\rho} \frac{\partial}{\partial \rho} \left(\rho \frac{\partial}{\partial \rho} B_z \right) - \frac{m^2}{\rho^2} B_z \right] \right\} = 0, \qquad (2.9)$$

and

$$\left(\frac{iq_0 \gamma_1^2}{\gamma_3^4} \right) \left\{ \left(\frac{kq_0 \epsilon_2}{\gamma_1^2} \right) \left[\frac{1}{\rho} \frac{\partial}{\partial \rho} \left(\rho \frac{\partial}{\partial \rho} E_z \right) - \frac{m^2}{\rho^2} E_z \right] \right.$$
$$\left. - \left[\frac{1}{\rho} \frac{\partial}{\partial \rho} \left(\rho \frac{\partial}{\partial \rho} B_z \right) + \left(\frac{\gamma_3^4}{\gamma_1^2} - \frac{m^2}{\rho^2} \right) B_z \right] \right\} = 0. \qquad (2.10)$$

Next, try a solution of the form of

$$E_z = a J_m(\beta \rho)$$
$$B_z = b J_m(\beta \rho) \qquad (2.11)$$

This gives an expression for β as follows:

$$\left(\frac{\epsilon_3 \gamma_3^4}{\epsilon_1 \gamma_2^2} - \beta^2 \right) \left(\frac{\gamma_3^4}{\gamma_1^2} - \beta^2 \right) + \left(\frac{k^2 q_0^2 \epsilon_2^2}{\epsilon_1 \gamma_2^2 \gamma_1^2} \right) \beta^4 = 0, \qquad (2.12)$$

where, for each of the two solutions β_i^2 $(i = 1, 2)$,

$$\frac{b_i}{a_i} = \frac{kq_0 \epsilon_2}{\gamma_3^4 - \gamma_1^2 \beta_i^2} \beta_i^2, \quad \text{or} \quad \frac{a_i}{b_i} = \frac{kq_0 \epsilon_2}{\epsilon_3 \gamma_3^4 - \epsilon_1 \gamma_2^2 \beta_i^2} \beta_i^2. \qquad (2.13)$$

The general solutions will, of course, be in the form of

$$E_z = a_1 J_m(\beta_1 \rho) + a_2 J_m(\beta_2 \rho)$$
$$B_z = b_1 J_m(\beta_1 \rho) + b_2 J_m(\beta_2 \rho). \quad (2.14)$$

Next, let $\vec{r} \equiv (\rho, \theta)$, $\vec{r}' \equiv (\rho', \theta')$, and define Green-function as

$$G(\vec{r}, \vec{r}') \equiv G(|\vec{r} - \vec{r}'|) \equiv G(\rho, \theta; \rho', \theta')$$
$$\equiv \sum_{m=-\infty}^{\infty} e^{im(\theta - \theta')} G(m; \rho, \rho'), \quad (2.15)$$

for the homogeneous (bulk) medium [see Eqs. (2.9) and (2.10)] as

$$\begin{bmatrix} \left[-\left(\dfrac{q_0^2 \epsilon_1 \gamma_2^2}{\gamma_3^4}\right)\left[\dfrac{1}{\rho}\dfrac{\partial}{\partial \rho}\left(\rho\dfrac{\partial}{\partial \rho}\right) + \left(\dfrac{\epsilon_3 \gamma_3^4}{\epsilon_1 \gamma_2^2} - \dfrac{m^2}{\rho^2}\right)\right] & -\left(\dfrac{q_0^2 \epsilon_1 \gamma_2^2}{\gamma_3^4}\right)\left(\dfrac{kq_0 \epsilon_2}{\epsilon_1 \gamma_2^2}\right)\left[\dfrac{1}{\rho}\dfrac{\partial}{\partial \rho}\left(\rho\dfrac{\partial}{\partial \rho}\right) - \dfrac{m^2}{\rho^2}\right] \\[4mm] \left(\dfrac{q_0^2 \gamma_1^2}{\gamma_3^4}\right)\left(\dfrac{kq_0 \epsilon_2}{\gamma_1^2}\right)\left[\dfrac{1}{\rho}\dfrac{\partial}{\partial \rho}\left(\rho\dfrac{\partial}{\partial \rho}\right) - \dfrac{m^2}{\rho^2}\right] & -\left(\dfrac{q_0^2 \gamma_1^2}{\gamma_3^4}\right)\left[\dfrac{1}{\rho}\dfrac{\partial}{\partial \rho}\left(\rho\dfrac{\partial}{\partial \rho}\right) + \left(\dfrac{\gamma_3^4}{\gamma_1^2} - \dfrac{m^2}{\rho^2}\right)\right] \end{bmatrix} \times \begin{bmatrix} G_{11}(m;\rho,\rho') & G_{12}(m;\rho,\rho') \\ G_{21}(m;\rho,\rho') & G_{22}(m;\rho,\rho') \end{bmatrix}$$

$$= -\frac{2}{\rho}\delta(\rho - \rho')\begin{bmatrix} 1 & 0 \\ 0 & 1 \end{bmatrix}. \quad (2.16)$$

We attempt a solution of the following form [see Ref. 22]:

$$G_{11}(m;\rho,\rho') = i\pi \begin{cases} a_1 J_m(\beta_1 \rho) H_m(\beta_1 \rho') + a_2 J_m(\beta_2 \rho) H_m(\beta_2 \rho'), & \rho \leq \rho' \\ a_1 H_m(\beta_1 \rho) J_m(\beta_1 \rho') + a_2 H_m(\beta_2 \rho) J_m(\beta_2 \rho'), & \rho \geq \rho', \end{cases} \quad (2.17)$$

$$G_{21}(m;\rho,\rho') = i\pi \begin{cases} b_1 J_m(\beta_1 \rho) H_m(\beta_1 \rho') + b_2 J_m(\beta_2 \rho) H_m(\beta_2 \rho'), & \rho \leq \rho' \\ b_1 H_m(\beta_1 \rho) J_m(\beta_1 \rho') + b_2 H_m(\beta_2 \rho) J_m(\beta_2 \rho'), & \rho \geq \rho' \end{cases}, \quad (2.18)$$

$$G_{12}(m;\rho,\rho') = i\pi \begin{cases} c_1 J_m(\beta_1 \rho) H_m(\beta_1 \rho') + c_2 J_m(\beta_2 \rho) H_m(\beta_2 \rho'), & \rho \leq \rho' \\ c_1 H_m(\beta_1 \rho) J_m(\beta_1 \rho') + c_2 H_m(\beta_2 \rho) J_m(\beta_2 \rho'), & \rho \geq \rho' \end{cases}, \quad (2.19)$$

$$G_{22}(m;\rho,\rho') = i\pi \begin{cases} d_1 J_m(\beta_1 \rho) H_m(\beta_1 \rho') + d_2 J_m(\beta_2 \rho) H_m(\beta_2 \rho'), & \rho \leq \rho' \\ d_1 H_m(\beta_1 \rho) J_m(\beta_1 \rho') + d_2 H_m(\beta_2 \rho) J_m(\beta_2 \rho'), & \rho \geq \rho' \end{cases}. \quad (2.20)$$

Let us note, for the moment, that both solutions for G_{11}, for example, can be combined together in the following form:

$$G_{11} = i\pi \{[1 - \theta(\rho - \rho')][a_1 J_m H_m + a_2 J_m H_m] + \theta(\rho - \rho')[a_1 H_m J_m + a_2 H_m J_m]\}, \quad (2.21)$$

where $\theta(x) = 1(0)$ for $x > 0 (x < 0)$ is the Heaviside step function. It is relatively involved, but straightforward, to verify step-by-step that Eqs. (2.17)–(2.20) represent the correct and exact solutions of Eq. (2.16). For the sake of simplicity and convenience, we redefine the coefficients involved in the elements of the Green-function matrix $\tilde{G}$ such that

$$C_{11} G_{11}(m;\rho,\rho') = i\pi \begin{cases} A_1 J_m(\beta_1 \rho) H_m(\beta_1 \rho') + A_2 J_m(\beta_2 \rho) H_m(\beta_2 \rho'), & \rho \leq \rho' \\ A_1 H_m(\beta_1 \rho) J_m(\beta_1 \rho') + A_2 H_m(\beta_2 \rho) J_m(\beta_2 \rho'), & \rho \geq \rho' \end{cases}, \quad (2.22)$$

$$C_{21} G_{21}(m;\rho,\rho') = i\pi \begin{cases} B_1 J_m(\beta_1 \rho) H_m(\beta_1 \rho') + B_2 J_m(\beta_2 \rho) H_m(\beta_2 \rho'), & \rho \leq \rho' \\ B_1 H_m(\beta_1 \rho) J_m(\beta_1 \rho') + B_2 H_m(\beta_2 \rho) J_m(\beta_2 \rho'), & \rho \geq \rho' \end{cases}, \quad (2.23)$$

$$C_{12} G_{12}(m;\rho,\rho') = i\pi \begin{cases} C_1 J_m(\beta_1 \rho) H_m(\beta_1 \rho') + C_2 J_m(\beta_2 \rho) H_m(\beta_2 \rho'), & \rho \leq \rho' \\ C_1 H_m(\beta_1 \rho) J_m(\beta_1 \rho') + C_2 H_m(\beta_2 \rho) J_m(\beta_2 \rho'), & \rho \geq \rho' \end{cases}, \quad (2.24)$$

$$C_{22} G_{22}(m;\rho,\rho') = i\pi \begin{cases} D_1 J_m(\beta_1 \rho) H_m(\beta_1 \rho') + D_2 J_m(\beta_2 \rho) H_m(\beta_2 \rho'), & \rho \leq \rho' \\ D_1 H_m(\beta_1 \rho) J_m(\beta_1 \rho') + D_2 H_m(\beta_2 \rho) J_m(\beta_2 \rho'), & \rho \geq \rho' \end{cases}. \quad (2.25)$$

Before we define the coefficients A_i, B_i, C_i, and D_i, it is quite important to employ following substitutions in order to make it simpler for the rest of the job to be done. These are $P_1 = \epsilon_3 \gamma_3^4/(\epsilon_1 \gamma_2^2)$, $P_2 = \gamma_3^4/\gamma_1^2$, $x_1 = kq_0\epsilon_2/(\epsilon_1 \gamma_2^2)$, and $x_2 = kq_0\epsilon_2/\gamma_1^2$. Thus the coefficients A_i, B_i, C_i, and D_i needed to redefine the bulk Green-functions [in the light of the prefactors involved in Eq. (2.16)] in Eqs. (2.22)–(2.25) take the following forms: $A_1 = -(P_2-\beta_1^2)/Z$, $A_2 = (P_2-\beta_2^2)/Z$, $B_1 = -\beta_1^2/Z$, $B_2 = \beta_2^2/Z$, $C_1 = -\beta_1^2/Z$, $C_2 = \beta_2^2/Z$, $D_1 = -(P_1-\beta_1^2)/Z$, and $D_2 = (P_1-\beta_2^2)/Z$, where $Z=MS$, with $M=(1+x_1x_2)$ and $S=(\beta_1^2-\beta_2^2)$. Here $C_{11} = -q_0^2\epsilon_1\gamma_2^2/\gamma_3^4$, $C_{21} = q_0^2\gamma_1^2/(\gamma_3^4 x_1)$, $C_{12} = -q_0^2\epsilon_1\gamma_2^2/(\gamma_3^4 x_2)$, and $C_{22} = -q_0^2\gamma_1^2/\gamma_3^4$. Then Eq. (2.12) assumes the following form:

$$(1+x_1x_2)\beta^4 - (P_1+P_2)\beta^2 + P_1P_2 = 0, \qquad (2.26)$$

and hence the two solutions of this equation are defined such that

$$\beta_{1,2}^2 = \frac{1}{2M}[(P_1+P_2) \pm \sqrt{(P_1-P_2)^2 - 4P_1P_2x_1x_2}]. \qquad (2.27)$$

It is important to note that $\beta_j = \pm i\delta_j$, with $j \equiv 1,2$, where δ_j represents the conventional definition of the decay constants in the Faraday geometry and can easily be recovered from Eq. (2.1). To be explicit, δ_j are given by[1]

$$\delta_{1,2}^2 = \frac{1}{2\epsilon_1}([(\epsilon_1+\epsilon_3)k_1^2 - q_0^2\epsilon_2^2]$$
$$\pm \sqrt{\{[(\epsilon_1-\epsilon_3)k_1^2 - q_0^2\epsilon_2^2]^2 - 4k^2q_0^2\epsilon_3\epsilon_2^2\}}). \quad (2.28)$$

For the sake of completeness, numerous identities interrelating x_i, γ_i, β_i, P_i, and M are relegated to Appendix B. In what follows, we will consider three types of perturbative operations to have the desired results for the response functions for the resultant system at hand. In doing so, we will recall the outlines of and abide by the conceptual scheme of interface response theory.[13]

III. FORMALISM FOR INVERSE RESPONSE FUNCTIONS

In this section, we will consider three perturbative operations represented geometrically by Fig. 1. Specifically, Fig. 1(a)–1(c) correspond, respectively, to the plasma cylinder of radius R_1 surrounded by a black box surface, a black box cylinder of radius R_2 surrounded by a plasma medium, and a plasma shell sandwiched between the black box cylinder of radius R_1 and a semi-infinite black box surface outside a cylinder of radius R_2. The plasma media in the perturbations 1(a)–1(c) are, in general, characterized by the local dielectric functions $\epsilon_1(\omega,B)$, $\epsilon_2(\omega,B)$, and $\epsilon_3(\omega,B)$, respectively (see Apendix A). We will consider the effect of retardation but neglect the absorption throught. Any subscript $i \equiv 1$, 2, or 3 on the physical quantities should be understood to refer to the respective perturbation until and unless stated otherwise.

Before proceeding to the specific details for the respective perturbations, we would like to enlist some of the important substitutions to be made in what follows. These are S_{j1}

$= \epsilon_{j1}\gamma_{j2}^2/\gamma_{j3}^2$, $S_{j2} = imk^2\epsilon_{j2}/(\epsilon_{j1}\gamma_{j2}^2)$, $S_{j3} = kq_0\epsilon_{j2}/(\epsilon_{j1}\gamma_{j2}^2)$, $S_{j4} = imk\gamma_{j1}^2/(q_0\epsilon_{j1}\gamma_{j2}^2)$, $S_{j5} = \gamma_{j1}^2/\gamma_{j3}^2$, $S_{j6} = kq_0\epsilon_{j2}/\gamma_{j1}^2$, $S_{j7} = imk/(q_0)$, and $S_{j8} = imq_0^2\epsilon_{j2}/(\gamma_{j1}^2)$. Here the letter j in the subscripts refers to the specific perturbation in question. At the same time, it is necessary to remember that all the quantities that are inherently involved inside these substitutions, such as, for example, x_i, γ_i, β_i, and P_i will also carry a similar additional first index j in their subscripts.

A. Brief strategy of the methodology

In order to avoid expanding on the mathematical details later, we would like to recall briefly some important outlines of the theoretical scheme of the interface response theory. It should be noted first that all the quantities referred to earlier or to be referenced in what follows will carry a subscript j when referring to a given perturbative operation. The first and the foremost point is to create a black-box surface in order to confine ourselves within the building block of the system and disconnect altogether from the rest of the mathematical world. For this purpose, we assume a step function $\theta(\cdots)$ specifying a given physical situation in front of Eqs. (2.2)–(2.5), for example. This then leads us to define a cleavage operator $\tilde{V}_j(\cdots)$ with the help of Eqs. (2.6) and (2.7), for example, which is, in fact, a $2n \times 2n$ matrix, where n is the number of interfaces in question. Now we also know beforehand that there is a bulk Green-function matrix $\tilde{G}_j(\cdots)$ representing the medium we are confined to. With this, we define a response operator,

$$\tilde{A}_j(\cdots) = \tilde{V}_j(\cdots)\tilde{G}_j(\cdots). \qquad (3.1)$$

The arguments of all of these matrices are many, depending upon the physical problem at hand, but the two that are the
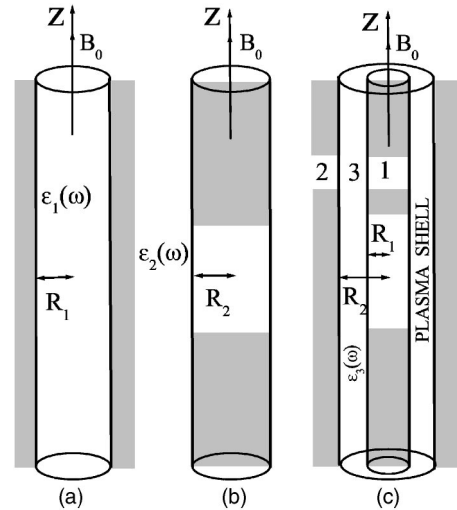

FIG. 1. Schematics of the concept of three perturbations: [A], [B], and [C]. The blank (shaded) region refers to the material medium (black box) in the system. The sum of the first two perturbations defines a plasma (dielectric) cylinder embedded in a dielectric (plasma) and the sum of all three perturbations specifies, say, a plasma (dielectric) shell surrounded by two unidentical dielectrics (plasmas). The magnetic field ($\vec{B}$) is oriented along the $\hat{z}$ axis of the cylinder.

most important to be specified are ρ and ρ' in the present problem, for example. Evidently, the response operator is also a $2n \times 2n$ matrix. Next, we define an operator,

$$\widetilde{\Delta}_j(\cdots) = \widetilde{I} + \widetilde{A}_j(\cdots), \qquad (3.2)$$

where $\widetilde{I}$ is a unit matrix of the same order as the rest. Now we need to calculate the inverse of the bulk Green-function $\widetilde{G}_j(\cdots)$, which is given by, say, $\widetilde{G}_j^{-1}(\cdots)$. As such, we now have all that we need to calculate the inverse response function $\widetilde{g}_j^{-1}(\cdots)$ in the interface space (say, M_s). This is defined by

$$\widetilde{g}_j^{-1}(\cdots) = \widetilde{\Delta}_j(\cdots)\widetilde{G}_j^{-1}(\cdots). \qquad (3.3)$$

Notice that $\widetilde{g}_j^{-1}(\cdots)$ represents *exclusively* the response function of the region we initially confined ourselves to, and that it does not yet stand for the physical system we may be interested in. To be more explicit, suppose that $\widetilde{g}_1^{-1}(\cdots)$ in Eq. (3.3) represents the dielectric, metallic, or semiconducting cylinder surrounded by a black box. And suppose we are interested in a physical system made up of this cylinder surrounded by a real, but different, material. Then we would have to follow the identical [to those leading to Eq. (3.3)] steps, but now we confine ourselves to the semi-infinite region enclosing the black box. Suppose the latter system turns out to be represented by an inverse response function $\widetilde{g}_2^{-1}(\cdots)$. Then our actual, final, physical system, say, made up of a semiconducting cylinder surrounded by a dielectric, is represented by

$$\widetilde{g}_f^{-1}(\cdots) = \widetilde{g}_1^{-1}(\cdots) + \widetilde{g}_2^{-1}(\cdots). \qquad (3.4)$$

This response function $\widetilde{g}_f^{-1}(\cdots)$ serves many useful purposes in realistic situations. For instance, the determinant of $\widetilde{g}_f^{-1}(\cdots)$ equated to zero yields the respective dispersive modes of, for example, a semiconducting cylinder surrounded by a semi-infinite dielectric. It also becomes useful to calculate the local as well as total density of states (see Sec. III F below). The analogous response functions are also useful to compute numerous electronic, optical, and vibrational properties of a given system under diverse physical situations. Such is the strategy of the IRT to be pursued in what follows for the specific system we are interested in here. As one can notice, one of the most important advantages of IRT over other classical or semiclassical theoretical schemes is that one does not need to match the messy boundary conditions one is so routinely used to in handling the inhomogeneous systems.

B. First perturbation

The first perturbation [represented by Fig. 1(a)] is specified by a step function $\theta(R_1 - \rho)$ in front of Eqs. (2.2)–(2.5). That means that the black-box cleavage operator $\widetilde{V}_1(R_1, \rho')$ is defined such that [see Eqs. (2.6) and (2.7)]

$\widetilde{V}_1(R_1, \rho')$

$$= \frac{R_1}{2} \frac{q_0^2}{\gamma_{13}^2} \begin{bmatrix} -S_{11}\left(\dfrac{\partial}{\partial \rho'} - \dfrac{1}{\rho'} S_{12}\right) & -S_{11}\left(S_{13}\dfrac{\partial}{\partial \rho'} + \dfrac{1}{\rho'} S_{14}\right) \\ S_{15}\left(S_{16}\dfrac{\partial}{\partial \rho'} + \dfrac{1}{\rho'} S_{17}\right) & -S_{15}\left(\dfrac{\partial}{\partial \rho'} - \dfrac{1}{\rho'} S_{18}\right) \end{bmatrix}$$

$$\times \delta(R_1 - \rho'), \qquad (3.5)$$

and the corresponding bulk Green-function is written as [see Eqs. (2.22)–(2.25)]

$$\widetilde{G}_1(\rho, \rho') = i\pi \frac{\gamma_{13}^2}{q_0^2} \begin{bmatrix} G_1(11) & G_1(12) \\ G_1(21) & G_1(22) \end{bmatrix}. \qquad (3.6)$$

It is noteworthy that although the operators $\widetilde{V}_1$ and $\widetilde{A}_1$ as well as the functions $\widetilde{G}_1$ and $\widetilde{g}_1$ are all functions of the variables, such as m, k, ω, ω_p, and ω_c, we have suppressed them throughout for the sake of brevity and convenience. The matrix elements $G_1(ij)$ are relegated to Appendix C. With this, we define the response operator,

$$\widetilde{A}_1(R_1, R_1) = \widetilde{V}_1(R_1, \rho)\widetilde{G}_1(\rho, \rho')\big|_{\rho = R_1 = \rho'}$$

$$= \frac{i\pi}{2M_1 S_1} \begin{bmatrix} A_1(11) & A_1(12) \\ A_1(21) & A_1(22) \end{bmatrix}. \qquad (3.7)$$

The matrix elements $A_1(ij)$ are relegated to Appendix C. Next we define an operator,

$$\widetilde{\Delta}_1(R_1, R_1) = \widetilde{I} + \widetilde{A}_1(R_1, R_1) = \frac{i\pi}{2M_1 S_1} \begin{bmatrix} \Delta_1(11) & \Delta_1(12) \\ \Delta_1(21) & \Delta_1(22) \end{bmatrix}. \qquad (3.8)$$

The matrix elements $\Delta_1(ij)$ are relegated to Appendix C. It should be pointed out that in writing the second equality in Eq. (3.8), we made a rigorous use of the identity in Eq. (B11) (see Appendix B).[23] Next, we calculate the inverse of $\widetilde{G}_1$ to write

$$\widetilde{G}_1^{-1}(R_1, R_1) = -\frac{iq_0^2 \epsilon_{11}}{\pi \gamma_{13}^2} \frac{1}{H_m(z_{11})J_m(z_{11})H_m(z_{12})J_m(z_{12})}$$

$$\times \begin{bmatrix} G_1(22) & -G_1(12) \\ -G_1(21) & G_1(11) \end{bmatrix}, \qquad (3.9)$$

where $z_{1i} = \beta_{1i}R_1$, with $i \equiv 1, 2$. As such, we have all that we need to calculate the inverse response function in the interface space M_s defined by

$$\widetilde{g}_1^{-1}(R_1, R_1) = \widetilde{\Delta}_1(R_1, R_1)\widetilde{G}_1^{-1}(R_1, R_1). \qquad (3.10)$$

The result is that

$$\widetilde{g}_1^{-1}(R_1, R_1) = \frac{i\pi}{2} \frac{Q_1}{M_1 S_1} \begin{bmatrix} h_1(11) & h_1(12) \\ h_1(21) & h_1(22) \end{bmatrix}, \qquad (3.11)$$

represents the response function of a plasma cylinder surrounded by a black box. Here Q_1 is defined as follows:

$$Q_1 = -\frac{i}{\pi}\frac{q_0^2}{\gamma_{13}^2}S_{11}S_{15}\frac{M_1}{H_m(z_{11})J_m(z_{11})H_m(z_{12})J_m(z_{12})}.$$
(3.12)

The matrix elements $g_1(ij)$ are relegated to Appendix C.

C. Second perturbation

The second perturbation [represented by Fig. 1(b)] is specified by a step function $\theta(\rho-R_2)$ in front of Eqs. (2.2)–(2.5). Then the black-box cleavage operator $\tilde{V}_2(R_2,\rho')$ is defined such that [see Eqs. (2.6) and (2.7)]

$$\tilde{V}_2(R_2,\rho') = -\frac{R_2}{2}\frac{q_0^2}{\gamma_{23}^2}$$
$$\times\begin{bmatrix} -S_{21}\left(\dfrac{\partial}{\partial\rho'}-\dfrac{1}{\rho'}S_{22}\right) & -S_{21}\left(S_{23}\dfrac{\partial}{\partial\rho'}+\dfrac{1}{\rho'}S_{24}\right) \\ S_{25}\left(S_{26}\dfrac{\partial}{\partial\rho'}+\dfrac{1}{\rho'}S_{27}\right) & -S_{25}\left(\dfrac{\partial}{\partial\rho'}-\dfrac{1}{\rho'}S_{28}\right) \end{bmatrix}$$
$$\times\delta(\rho'-R_2),$$
(3.13)

and the corresponding bulk Green-function is written as [see Eqs. (2.22)–(2.25)]

$$\tilde{G}_2(\rho,\rho') = i\pi\frac{\gamma_{23}^2}{q_0^2}\begin{bmatrix} G_2(11) & G_2(12) \\ G_2(21) & G_2(22) \end{bmatrix}.$$
(3.14)

The matrix elements $G_2(ij)$ are relegated to Appendix D. With this, we define the response operator,

$$\tilde{A}_2(R_2,R_2) = \tilde{V}_2(R_2,\rho)\tilde{G}_2(\rho,\rho')\big|_{\rho=R_2=\rho'}$$
$$= -\frac{i\pi}{2M_2S_2}\begin{bmatrix} A_2(11) & A_2(12) \\ A_2(21) & A_2(22) \end{bmatrix}.$$
(3.15)

The matrix elements $A_2(ij)$ are relegated to Appendix D. Next we define an operator,

$$\tilde{\Delta}_2(R_2,R_2) = \tilde{I} + \tilde{A}_2(R_2,R_2) = -\frac{i\pi}{2M_2S_2}\begin{bmatrix} \Delta_2(11) & \Delta_2(12) \\ \Delta_2(21) & \Delta_2(22) \end{bmatrix}.$$
(3.16)

The matrix elements $\Delta_2(ij)$ are relegated to Appendix D. Again, in writing the second equality in Eq. (3.16), we have made a rigorous use of the identity in Eq. (B11) (see Appendix B). Next, we calculate the inverse of $\tilde{G}_2$ to write

$$\tilde{G}_2^{-1}(R_2,R_2) = -\frac{iq_0^2\epsilon_{21}}{\pi\gamma_{23}^2}\frac{1}{H_m(z_{21})J_m(z_{21})H_m(z_{22})J_m(z_{22})}$$
$$\times\begin{bmatrix} G_2(22) & -G_2(12) \\ -G_2(21) & G_2(11) \end{bmatrix},$$
(3.17)

where $z_{2i}=\beta_{2i}R_1$, with $i\equiv1,2$. As such, we have all that we need in order to calculate the inverse response function in the interface space M_s defined by

$$\tilde{g}_2^{-1}(R_2,R_2) = \tilde{\Delta}_2(R_2,R_2)\tilde{G}_2^{-1}(R_2,R_2).$$
(3.18)

The result is that

$$\tilde{g}_2^{-1}(R_2,R_2) = -\frac{i\pi}{2}\frac{Q_2}{M_2S_2}\begin{bmatrix} h_2(11) & h_2(12) \\ h_2(21) & h_2(22) \end{bmatrix}$$
(3.19)

represents the response function of a black-box cylinder surrounded by a plasma medium. Here Q_2 is defined as follows:

$$Q_2 = -\frac{i}{\pi}\frac{q_0^2}{\gamma_{23}^2}S_{21}S_{25}\frac{M_2}{H_m(z_{21})J_m(z_{21})H_m(z_{22})J_m(z_{22})}.$$
(3.20)

The matrix elements $g_2(ij)$ are relegated to Appendix D.

D. Third perturbation

The third perturbation [represented by Fig. 1(c)] is specified by a step function $[\theta(\rho-R_1)-\theta(\rho-R_2)]$ in front of Eqs. (2.2)–(2.5). Then the black-box cleavage operator $\tilde{V}_3(R_i,\rho')\delta(\rho'-R_i)P_{nn'}$ [with $P_{nn'}=1(0)$ for $n,n'\leq2$ and ≥3 (otherwise); $i=1$ (2) for $n,n'\leq2$ (≥3)] is defined such that

$$\tilde{V}_3(R_i,\rho') = \begin{bmatrix} \tilde{V}_{32} & \tilde{0} \\ \tilde{0} & \tilde{V}_{31} \end{bmatrix},$$
(3.21)

where $\tilde{V}_{32}=\tilde{V}_2$ [see Eq. (3.13)], with $R_2\to R_1$, $\gamma_{2i}\to\gamma_{3i}$ and $S_{2i}\to S_{3i}$, and $\tilde{V}_{31}=\tilde{V}_1$ [see Eq. (3.5)], with $R_1\to R_2$, $\gamma_{1i}\to\gamma_{3i}$, and $S_{1i}\to S_{3i}$.

The corresponding bulk Green-function is written as

$$\tilde{G}_3(M_s,M_s) = i\pi\frac{\gamma_{33}^2}{q_0^2}\begin{bmatrix} G_3(11) & G_3(12) & G_3(13) & G_3(14) \\ G_3(21) & G_3(22) & G_3(23) & G_3(24) \\ G_3(31) & G_3(32) & G_3(33) & G_3(34) \\ G_3(41) & G_3(42) & G_3(43) & G_3(44) \end{bmatrix},$$
(3.22)

where the interface space M_s will be referred to $(\rho=R_1,\rho'=R_1)$, $(\rho=R_1,\rho'=R_2)$, $(\rho=R_2,\rho'=R_2)$, and $(\rho=R_2,\rho'=R_1)$,

respectively, in the first, second, third, and fourth quadrants made up of 2×2 submatrices, starting clockwise from the top-left quadrant. The matrix elements $G_3(ij)$ are relegated to Appendix E. With this, we define the response operator,

$$\widetilde{A}_3(M_s,M_s) = \widetilde{V}_3(M_s)\widetilde{G}_3(M_s,M_s)$$

$$= \frac{i\pi}{2M_3S_3}\begin{bmatrix} A_3(11) & A_3(12) & A_3(13) & A_3(14) \\ A_3(21) & A_3(22) & A_3(23) & A_3(24) \\ A_3(31) & A_3(32) & A_3(33) & A_3(34) \\ A_3(41) & A_3(42) & A_3(43) & A_3(44) \end{bmatrix}.$$

(3.23)

The matrix elements $A_3(ij)$ are relegated to Appendix E. Now we define an operator,

$$\widetilde{\Delta}_3(M_s,M_s) = \widetilde{I} + \widetilde{A}_3(M_s,M_s)$$

$$= \frac{i\pi}{2M_3S_3}\begin{bmatrix} \Delta_3(11) & \Delta_3(12) & \Delta_3(13) & \Delta_3(14) \\ \Delta_3(21) & \Delta_3(22) & \Delta_3(23) & \Delta_3(24) \\ \Delta_3(31) & \Delta_3(32) & \Delta_3(33) & \Delta_3(34) \\ \Delta_3(41) & \Delta_3(42) & \Delta_3(43) & \Delta_3(44) \end{bmatrix}.$$

(3.24)

The matrix elements $\Delta_3(ij)$ are relegated to Appendix E. Again, in writing the second equality in Eq. (3.24), we have made use of the identity in Eq. (B11). Next, we calculate the inverse of the bulk Green-function $\widetilde{G}_3$ to write

$$\widetilde{G}_3^{-1}(M_s,M_s)$$

$$= -i\frac{q_0^2}{\pi\gamma_{33}^2}\frac{1}{D}$$

$$\times \begin{bmatrix} G_3^{-1}(11) & G_3^{-1}(12) & G_3^{-1}(13) & G_3^{-1}(14) \\ G_3^{-1}(21) & G_3^{-1}(22) & G_3^{-1}(23) & G_3^{-1}(24) \\ G_3^{-1}(31) & G_3^{-1}(32) & G_3^{-1}(33) & G_3^{-1}(34) \\ G_3^{-1}(41) & G_3^{-1}(42) & G_3^{-1}(43) & G_3^{-1}(44) \end{bmatrix},$$

(3.25)

where the matrix elements $G_3^{-1}(ij)$ are relegated to Appendix E and the symbol D is defined as follows:

$$D = \frac{S_3}{S_{31}S_{35}}[H_m(z_{31})J_m(z_{31}') - J_m(z_{31}')H_m(z_{31})]$$

$$\times [H_m(z_{32})J_m(z_{32}') - J_m(z_{32}')H_m(z_{32})]$$

$$\times J_m(z_{31})H_m(z_{32})J_m(z_{31}')H_m(z_{32}'),$$

(3.26)

where $z_{3i} = \beta_{3i}R_1$ and $z_{3i}' = \beta_{3i}R_2$. Finally, we calculate the inverse response function of a cylindrical shell bounded by two black boxes,

$$\widetilde{g}_3^{-1}(M_s,M_s) = \widetilde{\Delta}_3(M_s,M_s)\widetilde{G}_3^{-1}(M_s,M_s), \qquad (3.27)$$

to write

$$\widetilde{g}_3^{-1}(M_s,M_s) = \frac{1}{2}\frac{q_0^2}{\gamma_{33}^2}\frac{1}{S_3}\begin{bmatrix} h_3(11) & h_3(12) & h_3(13) & h_3(14) \\ h_3(21) & h_3(22) & h_3(23) & h_3(24) \\ h_3(31) & h_3(32) & h_3(33) & h_3(34) \\ h_3(41) & h_3(42) & h_3(43) & h_3(44) \end{bmatrix},$$

(3.28)

where the matrix elements $g_3(ij)$ are relegated to Appendix E. Having calculated the inverse response functions for the three perturbations, it becomes an easy task to deduce the dispersion relations for the plasmon propagation in the real physical systems. These are (i) a plasma (dielectric) cylinder embedded in a dielectric (plasma) and (ii) a plasma (dielectric) shell surrounded by two unidentical dielectrics (plasmas), for example. This is what we intend to do in what follows.

A step-by-step careful diagnosis of all the analytical results in this perturbation leads us to reproduce exactly the corresponding ones in the special limit of $B=0$ (cf. Ref. 19). This remark is also valid for other perturbations (in Secs. III B and III C. We recall and stress that we have, for the sake of generality, considered so far every physical medium in the first (Sec. III B), second (Sec. III C), and third (Sec. III D) perturbation to be a semiconducting plasma.

E. Plasma (dielectric) cylinder embedded in dielectric (plasma)

The merger of perturbations [Figs. 1(a) and 1(b)] results into a geometry of a plasma (dielectric) cylinder embedded in a dielectric (plasma), of course, with $\omega_p = 0 = \omega_c$ in the medium considered to be a dielectric. As such, one can write $\widetilde{g}^{-1} = \widetilde{g}_1^{-1} + \widetilde{g}_2^{-1}$, where $\widetilde{g}^{-1}$ is the inverse response function of a single cylinder embedded in a semi-infinite medium. That means that formally the determinant of the sum of the inverse response functions in Eqs. (3.11) and (3.19), with $R_1 = R = R_2$, equated to zero, i.e.,

$$|\widetilde{g}^{-1}(M_s,M_s)| = |\widetilde{g}_1^{-1}(M_s,M_s) + \widetilde{g}_2^{-1}(M_s,M_s)| = 0,$$

(3.29)

yields the dispersion relation for magnetoplasmons with a mixed (i.e., inseparable p- and s-polarizations) character in a single-interface cylindrical geometry. In order to gain confidence we subjected Eq. (3.29) to the limit of $R\rightarrow\infty$. The result is that a careful mathematical manipulation leaves us with an equation exactly identical to Eq. (45) in Ref. 24, which represents the dispersion relation for the magnetoplasmons propagating at an interface separating a semiconducting plasma and a dielectric. We also checked the limit of $B = 0$ everywhere in Eq. (3.29) to exactly reproduce our Eq. (3.27) in Ref. 19.

F. Plasma (dielectric) shell bounded by two unidentical dielectrics (plasmas)

In this section we are motivated to study a physical system made up of two coaxial cylinders where we can have the plasma shell bounded by two unidentical dielectrics or a dielectric shell bounded by two unidentical plasmas, in general. We will study diverse situations of practical interest.

Methodologically, such a geometry becomes realizable by summing up the inverse response functions calculated in Eqs. (3.11), (3.19), and (3.28) in the interface space M_s. One can write $\widetilde{g}^{-1} = \widetilde{g}_1^{-1} + \widetilde{g}_2^{-1} + \widetilde{g}_3^{-1}$, where $\widetilde{g}^{-1}$ is the response function of the finite cylindrical shell surrounded by two, in general, unidentical media. This implies that the following relation:

$$|\widetilde{g}^{-1}(M_s, M_s)| = |\widetilde{g}_1^{-1}(M_s, M_s) + \widetilde{g}_2^{-1}(M_s, M_s) + \widetilde{g}_3^{-1}(M_s, M_s)|$$
$$= 0 \qquad (3.30)$$

represents the dispersion relation for the magnetoplasmons in such a resultant two-interface coaxial, cylindrical structure where all the three physical media can, in principle, be different plasmas. However, such a situation would be too difficult to understand and interpret, given the fact that even if only one medium is magnetoplasma (in, say, a one-interface geometry) there can, in general, propagate *four* different kinds of modes [see, e.g., Ref. 1]. As such, we decided to study relatively more convenient situations such as, for example, (i) a plasma shell bounded by two identical dielectrics, (ii) a plasma shell bounded by two unidentical dielectrics, and (iii) a dielectric shell bounded by two identical plasmas. The term dielectric is literally used to mean a medium where the dielectric function is simply a *constant*, and hence the magnetic field has no influence whatsoever.

It should be pointed out that we performed two tests on the general analytical expression in Eq. (3.30) in the case of a geometry made up of a plasma shell bounded by two unidentical dielectrics. First, we consider the limit $R_1 \sim R_2 \sim R \rightarrow \infty$, but take $R_2 - R_1 = d$ as a finite quantity and fix $m = 0$. In this case a rigorous analytical diagnosis, which requires numerous identities listed in Appendix B, led us to exactly derive Eq. (19) in Ref. 25, which represents the magnetoplasmons in a semiconducting film bounded by two unidentical dielectrics. Second, we put the magnetic field $B = 0$ everywhere in Eq. (3.30) to reproduce exactly our Eq. (3.32) in Ref. 19.

Before closing this section, we would like to remark that in the numerical results (see Sec. IV) we will always come across a situation in which all the magnetoplasma modes at higher values of the propagation vector intend to be asymptotic to certain characteristic frequencies Ω_s. We have found that these characteristic frequencies turn out to be exactly the same as those in the case of a single- or double-interface planar geometry in the Faraday configuration (i.e., $\vec{B} \| \vec{k}$) and are specified by

$$\Omega_s^2 = \frac{1}{2[\epsilon_L^2 - \epsilon_0^2]}\{[(\epsilon_L^2 - \epsilon_0^2)\Omega_c^2 + 2\epsilon_L^2]$$
$$\pm [(\epsilon_L^2 - \epsilon_0^2)^2 \Omega_c^4 + 4\epsilon_L^2 \epsilon_0^2]^{1/2}\}, \qquad (3.31)$$

where ϵ_L is the background dielectric constant of the semiconducting plasma medium, ϵ_0 is the dielectric constant of the dielectric medium, and $\Omega_c = \omega_c/\omega_p$ is the normalized electron cyclotron frequency.

G. Local and total density of states

The density of states (DOS) is of fundamental importance to the understanding of many physical phenomena in condensed-matter physics. The interpretation of quite a number of experimental excitation spectra in a wide variety of systems subjected to different physical conditions requires a detailed knowledge of the DOS. The classic textbooks and monographs reveal that the standard algorithm to determine the density of states is founded on the Green-function approach. Our purpose here is to calculate the local and total DOS in order to substantiate the computed plasmon modes in the cylindrical geometries at hand. Unless some numeric hurdle gets in the way, it is logical to expect that the (positive) peaks in the DOS should coincide with the zeros of the inverse response function, which determine the plasmon modes for a given propagation vector of a system.

1. Local density of states

The formal expression for the local density of states (LDOS) in the framework of interface response theory is generally quite fussy, and as the name suggests requires some subtle details of the local physical conditions. These are, for example, the basic definitions of the bulk Green-functions, the spatial positions around the interface, the nature of the associated EM fields involved,…, etc. In the present context, the simplest definition of the LDOS at the expense of a few negligible concerns, but which still contains the important physics involved is given by[13]

$$\mathcal{N}_L(\omega) = -2\frac{\omega}{\pi}\text{Im}\{\text{trace}[\widetilde{g}(M_s, M_s)]\}, \qquad (3.32)$$

where $\widetilde{g}$ refers to the response function for which the inverse was determined in Secs. III B–III D for diverse situations. The important thing is to understand to which system the response function $\widetilde{g}$ refers in different physical situations. We consider two such cases of our interest: a single-interface system (see Sec. III E) and a double-interface system (see Sec. III F). For a single-interface system, $\widetilde{g}$ is simply the inverse of the sum of $\widetilde{g}_1^{-1}$ and $\widetilde{g}_2^{-1}$ (see Sec. III E). In the case of a two-interface system, we need to study the LDOS at the two interfaces R_1 and R_2 independently. For interface R_1 (R_2) the $\widetilde{g}$ in Eq. (3.32) is the 2×2 submatrix in the first (fourth) quadrant of the inverse of the sum of three inverse response functions (see Sec. III F).

2. Total density of states

For the z components of the electromagnetic fields considered here, the analytical expression for the variation of the total density of states (TDOS) within the interface response theory is given by[13]

$$\mathcal{N}_T(\omega) = -\frac{1}{\pi}\frac{d}{d\omega}\left(\text{Arg det}\left[\frac{\widetilde{g}_i(M_s, M_s)}{\widetilde{g}_f(M_s, M_s)}\right]\right). \qquad (3.33)$$

By the variation of TDOS we mean the difference between the TDOS of the final (physical) system and an initial system. Here $\widetilde{g}_i$ ($\widetilde{g}_f$) stands for the response function of the initial (final) system in question. For the single-interface sys-

tem, $\widetilde{g}_i$ is the product of $\widetilde{g}_1$ and $\widetilde{g}_2$; and $\widetilde{g}_f$ is the inverse of the sum of $\widetilde{g}_1^{-1}$ and $\widetilde{g}_2^{-1}$. In the case of a two-interface system, $\widetilde{g}_i = \widetilde{g}_{1f}\widetilde{g}_{2f}$, where $\widetilde{g}_{1f}$ is the inverse of the sum of a 4×4 matrix comprised of the $\widetilde{g}_1^{-1}$ and $\widetilde{g}_2^{-2}$, $\widetilde{g}_{2f}$ is the inverse of $\widetilde{g}_3^{-1}$ that corresponds to perturbation 3 for the shell alone, and $\widetilde{g}_f$ is the inverse of the sum of $\widetilde{g}_1^{-1}$, $\widetilde{g}_2^{-1}$, and $\widetilde{g}_3^{-1}$. It should be pointed out that both the local and total DOS are computed for every value of integer m.

It is also worth mentioning that in the course of studying the total DOS we have the finite (or bounded) parts of the system automatically incorporated. Therefore, we are bound to find some discrete modes in the TDOS, which usually apppear as negative peaks in the DOS-ω space and do not bear any physical significance if one is interested in studying only the confined or extended plasmon polaritons. Moreover, if we are interested in understanding all the existing peaks in the TDOS, we need to explore, for example, each of the three perturbations involved individually. We have found that while the negative peaks in the individual perturbations survive in the TDOS, all the positive peaks are seen to disappear. Moreover, all the (positive plus negative) peaks in a given perturbation are found to be well defined by the zeros of the respective inverse response function. This remains unfailingly true for all the cases we have investigated, both for single- and double-interface systems. All the peaks in the LDOS are always positive. More specific comments will be made later (see Sec. IV).

IV. ILLUSTRATIVE EXAMPLES

As we have seen in Sec. III, our final results for the magnetoplasmon dispersion characteristics are Eqs. (3.29) and (3.30), respectively, for the single cylinder embedded in a background of different material and the coaxial cylindrical geometries. Note that both of these equations are, in general, the complex transcendental functions. Therefore, in principle, we need to search the zeros of such complex functions. In spite of so many advancements in the software science, searching the reliable zeros of such complex functions is not an easy task. So, we strike a compromise among a few choices. We decided here to produce those zeros where the real part of the function changes the sign, irrespective of whether or not the imaginary part is zero. We believe that this has resulted into a reliable scheme for studying the dispersion characteristics of magnetoplasmons in the present systems. This is because all the magnetoplasma modes (confined or extended) are found to have excellent correspondence with the peaks in the local and/or total density of states. We consider mostly GaAs plasma, $Ga_{1-x}Al_xAs$ dielectric, and SiO_2 dielectric with background dielectric constants $\epsilon_L = 13.1$, 12.4, and 4.5, respectively. We will later assign an additional numeral to the suffix of the background dielectric constants corresponding to the region in the geometry concerned. Other parameters such as the aspect ratio $r = R_2/R_1$, the normalized plasma frequency $\Omega_p = \omega_p R_1/c$, the normalized electron-cyclotron frequency $\Omega_c = \omega_c/\omega_p$, and the azimuthal index of the Bessel functions m will be given at the appropriate places during the discussion. We will present our results in terms of the dimensionless propagation vector ζ
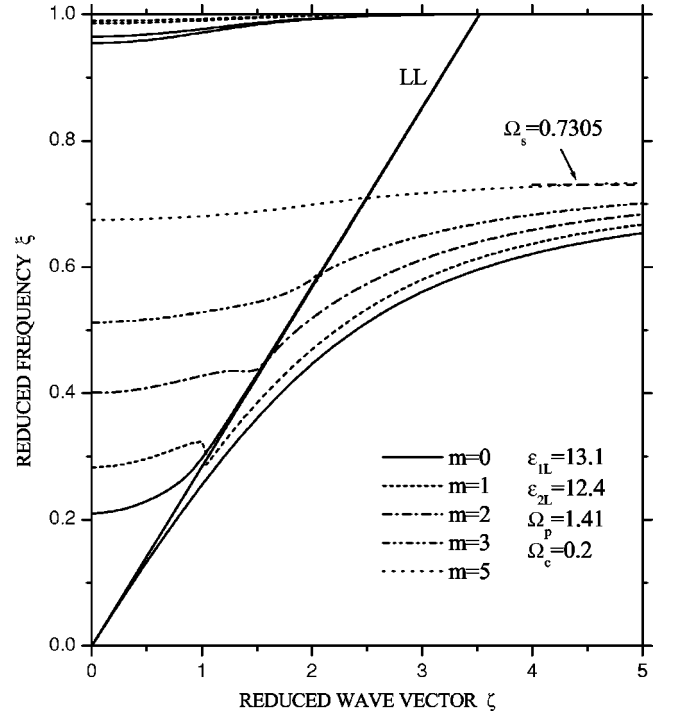

FIG. 2. Magnetoplasmon dispersion for a GaAs plasma cylinder ($\epsilon_{1L}=13.1$) embedded in a $Ga_{1-x}Al_xAs$ dielectric ($\epsilon_{2L}=12.4$). The other parameters are $\Omega_p=1.41$ and $\Omega_c=0.2$. The solid straight line marked as *LL* is the light line in the dielectric background. The dashed horizontal line refers to the asymptotic frequency $\xi = 0.7305$.

$= ck/\omega_p$ and frequency $\xi = \omega/\omega_p$, where ω_p stands for the screened plasma frequency. Both local and total DOS will be shown in arbitrary units throughout. It is important to note that we will henceforth label the *magnetic-field dependent (independent) decay constants by $\beta_\pm$ (β_j, with $j \equiv 1$, 2, or 3, referring to the number of the perturbation) just for the purpose of discussion.*

A. Plasma (dielectric) cylinder embedded in dielectric (plasma)

Figure 2 shows the plasmon dispersion for a GaAs plasma cylinder in the $Ga_{1-x}Al_xAs$ dielectric for $m=0$, 1, 2, 3, and 5 with $\Omega_p=1.41$. The dashed horizontal line marked as $\Omega_s = 0.7305$ indicates the corresponding asymptotic frequency Ω_s [see, for instance, Eq. (3.31)] in the nonretardation limit. The straight line marked as *LL* stands for the light line in the dielectric background. It is observed that there are two modes for every m: one starts in the radiative region (towards the left of the light line where β_2 is purely real) with a finite frequency, and the other starts at the origin along and towards the right of the light line in the non radiative region (towards the right of the light line where β_2 is purely imaginary). The former ends up merging with the light line, while the latter becomes asymptotic to $\xi = 0.7305$. This is the factual detail, albeit the picture apparently reveals something differently. A simple look at Fig. 2 makes us believe that there is one mode for every m that starts with a finite ξ from
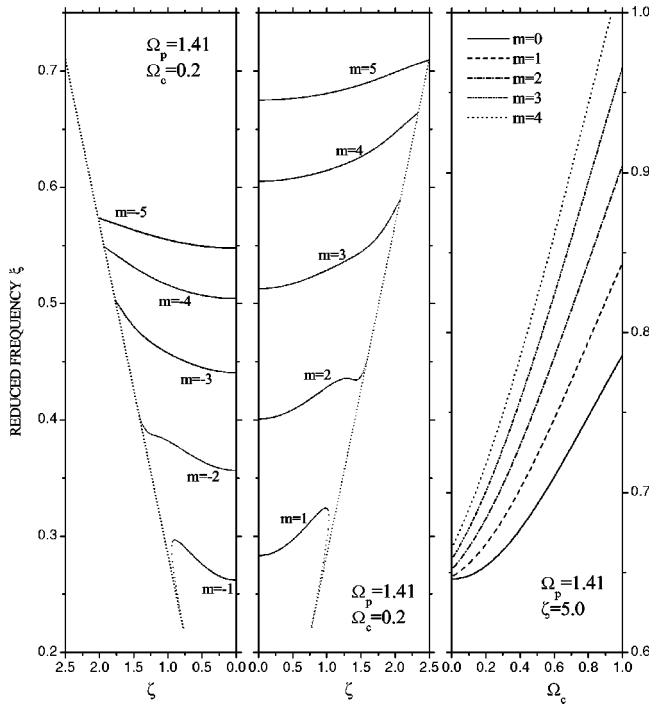
FIG. 3. Nonreciprocal behavior for the magnetoplasmon dispersion for a GaAs plasma cylinder embedded in a $Ga_{1-x}Al_xAs$ dielectric. The other parameters are listed inside the picture. The left panel shows the dispersion for $m<0$, the middle panel shows the dispersion for $m>0$, and the right panel shows the effect of the variation of the magnetic field intensity Ω_c for a given ζ.

FIG. 4. Local (total) density of states in the upper (lower) panel for various values of m and $\zeta=2.5$. The rest of the parameters used are the same as in Fig. 2. The arrow in the lower panel refers to a small invisible negative peak at $\xi=0.7100$ for $m=0$ where $\beta_2=0$.

$\zeta=0$ in the radiative region, propagates monotonously to take a small dip (at least for smaller m) in the close vicinity of the light line, and gradually tends to become asymptotic to Ω_s. The only exception to this description is the case of $m=0$, where the actual bona fide mode starts from the origin and is seen to be always the true magnetoplasmon polariton. Even at considerably large ζ, all modes retain their character: the larger the m, the higher the frequency. We see some additional modes for $m=0$ and $m=1$ in the close vicinity of the plasma frequency $\xi=1$.

The triptych in Fig. 3 is made up of three parts: the left part shows the dispersion characteristics for negative m, the middle part shows the dispersion for positive m, and the right part depicts the influence of the variation of intensity of the applied magnetic field for a given propagation vector ζ. Most of the parameters used here are the same as in Fig. 2, and we cover only the radiative regions, where the nonreciprocity is predominant. Just as it is expected intuitively, it becomes clear from the left and middle parts of this triptych that the magnetoplasma wave propagation in a semiconducting cylinder embedded in a dielectric in the presence of an applied magnetic field in the Faraday geometry is non reciprocal with respect to the change of the sign of the index m of the Bessel functions, i.e., $\xi(m>0) \neq \xi(m<0)$. Note that the nonreciprocity is found to be a general characteristic of the magnetoplasmon propagation in the cylindrical geometries in the presence of an applied magnetic field in the Faraday configuration. The right part clearly demonstrates the monotonous increase of the magnetoplasma frequency with the magnetic
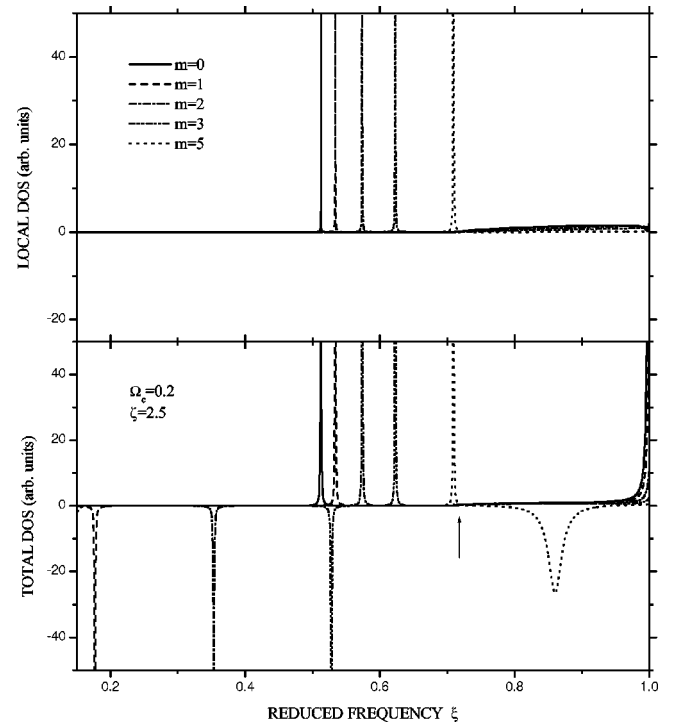
field intensity. But it should be noted that this behavior is shown for a given value of ζ. However, all the modes at any value of B do show a correct asymptotic behavior specified by Eq. (3.31).

Figure 4 illustrates the local (total) density of states in the upper (lower) panel in the nonradiative region in the $\xi-\zeta$ space for $m=0$, 1, 2, 3, and 5 and for $\zeta=2.5$. The rest of the parameters are the same as in Fig. 2. The sharp peaks at $\xi =0.5124$, 0.5339, 0.5738, 0.6230, and 0.7094 are seen to be common to both local and total DOS. The negative peaks are coming from the second perturbation (see Sec. III), which produces one positive and another negative peak for every m. The positive peak disappears and the negative one survives in the total DOS. The arrow at $\xi=0.7100$ indicates an indiscernibly small negative peak for $m=0$, where β_2 vanishes. We observe a pileup of rather small DOS, both local and total, at $\xi \geqslant 0.7305$. Every positive peak in the local and/or total DOS shows an excellent correspondence with the respective confined magnetoplasmon mode (in the nonradiative region) in Fig. 2. Let us clarify once and for all that these negative peaks in the total DOS are shown just for completeness, but really have no physical significance.

Figure 5 depicts the plasmon dispersion for a $Ga_{1-x}Al_xAs$ cylinder embedded in a GaAs plasma for $\Omega_p=1.41$ and $\Omega_c =0.2$. The solid, dashed, dashed-dotted, dashed-dot-dotted, and dotted curves stand for the magnetoplasmon modes, respectively, for $m=0$, 1, 2, 3, and 5. The dashed line marked as $\xi=0.7305$ refers to its asymptotic frequency in the nonretardation limit. Unlike as in Fig. 2, we observe a larger number of extended modes (in the region towards the left of the
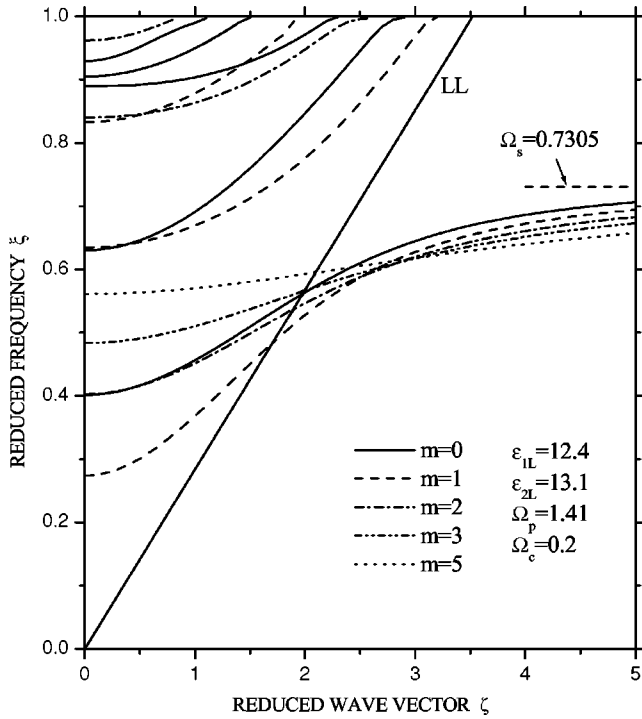
FIG. 5. Magnetoplasmon dispersion for a $Ga_{1-x}Al_xAs$ dielectric ($\epsilon_{1L}=12.4$) in GaAs plasma ($\epsilon_{2L}=13.1$). There are five groups of curves for five different values of m. The parameters used are as listed in the figure.
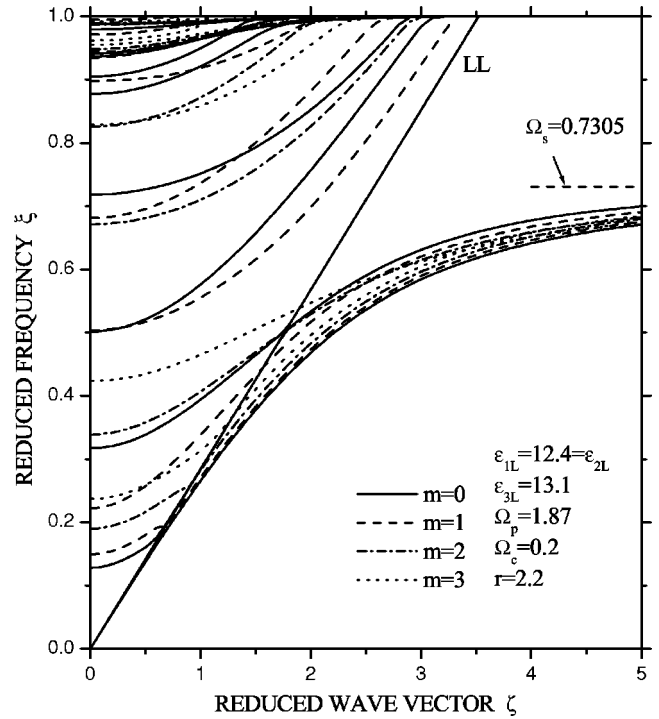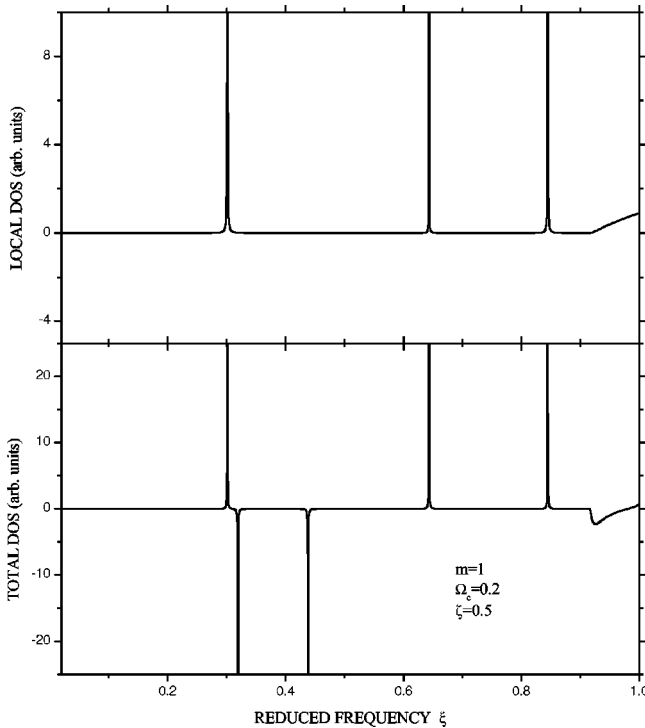

FIG. 7. Magnetoplasmon dispersion in a GaAs plasma ($\epsilon_{3L}=13.1$) shell sandwiched between identical $Ga_{1-x}Al_xAs$ dielectrics ($\epsilon_{1L}=12.4=\epsilon_{2L}$). There are five groups of curves for five different values of m. The solid, straight line labeled as LL refers to the light line in the $Ga_{1-x}Al_xAs$ dielectrics. The parameters used in the computation are as listed in the picture.

FIG. 6. Local (total) density of states in the upper (lower) panel for $m=1$ and $\zeta=0.5$. The rest of the parameters used are the same as in Fig. 5. The negative peaks in the lower panel emerge from the first perturbation alone and bear no physical significance.

light line marked as LL) for every m, even though the number of confined magnetoplasmons at large ζ is still the same (i.e., one for every m). It is interesting to note that in the present case there is almost a smooth transition of the magnetoplasmon propagation in the vicinity of the light line. This contrasts with the corresponding behavior in Fig. 2. Another important difference is the fact that all the confined modes seem to merge together and lose their identities—with respect to (nonzero) index m—at some characteristic value of ζ (see, for example, at $\zeta \simeq 2.75$). This kind of *focusing* effect, which is more explicit for this geometry than in others (see, e.g., Sec. V), could possibly be explored to characterize the materials constituting the resultant structure.

Figure 6 shows the local (total) density of states in the upper (lower) panel for $m=1$ and $\zeta=0.5$. The other parameters are the same as in Fig. 5. All three positive peaks appearing at $\xi=0.3012$, 0.6435, and 0.8446 in the local DOS are seen to be consistent with the corresponding positive peaks in the total DOS. These positive peaks showing up in the local and total DOS are seen to be in very good agreement with the frequencies of the three radiative plasmon modes at $\zeta=0.5$ in Fig. 5. The existence of the two negative peaks at $\xi=0.3190$ and 0.4381 in the total DOS is attributed to the first perturbation alone. It is found that both of the negative peaks are the exact solutions of $|\tilde{g}_1^{-1}|=0$. Moreover, the positive peaks occurring at $\xi=0.1420$ and 0.7824 (where J_1 vanishes) in the first perturbation are seen to disappear from the total DOS.
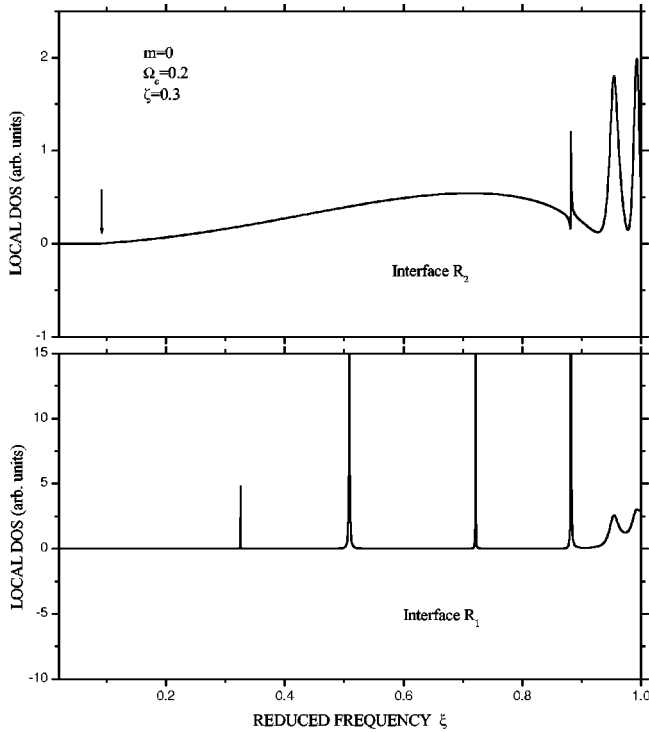
FIG. 8. Local density of states at the interface R_1 (R_2) in the lower (upper) panel for $m=0$ and $\zeta=0.3$. We call attention to the smaller DOS resonance, (indicated by the arrow), corresponding to the interface R_2. The rest of the parameters used are the same as in Fig. 7.

B. Plasma (dielectric) shell bounded by two dielectrics (plasmas)

Figure 7 illustrates the dispersion relations of the magnetoplasmon-polariton modes for the coaxial cylindrical geometry made up of a GaAs plasma shell bounded by the $Ga_{1-x}Al_xAs$ dielectrics, both in the inner cylinder and the outer semi-infinite medium. As for other relevant parameters, we consider $\Omega_p=1.87$, $\Omega_c=0.2$, and $r=2.2$. The solid, dashed, dashed-dotted, and dotted curves stand for the values of $m=0$, 1, 2, and 3. Since the inner and outer media are identical, we still have a single asymptotic frequency in the nonretardation limit $\xi=0.7305$ assigned to the dashed horizontal line. The straight, solid line marked as LL is the light line in the $Ga_{1-x}Al_xAs$ dielectrics enclosing the plasma shell. Note that while the number of the confined magnetoplasmon modes at large value of ζ (in the nonradiative region) is still two in conformation with the two interfaces in question, there can be any number of extended modes in the radiative region for a given m, depending upon the aspect ratio r. The upper, confined magnetoplasmons at $\zeta \simeq 2.65$ demonstrate the same kind of *focusing* effect as observed in Fig. 5. An additional effect of the presence of the magnetic field is the accumulation of the radiative modes near the plasma frequency at $\zeta \lesssim 2.2$.

Figure 8 shows the local density of states at the interface R_1 (R_2) in the lower (upper) panel for $m=0$ and $\zeta=0.3$. The rest of the parameters are the same as in Fig. 7. We note that there are four well-defined sharp DOS peaks at $\xi=0.3252$,
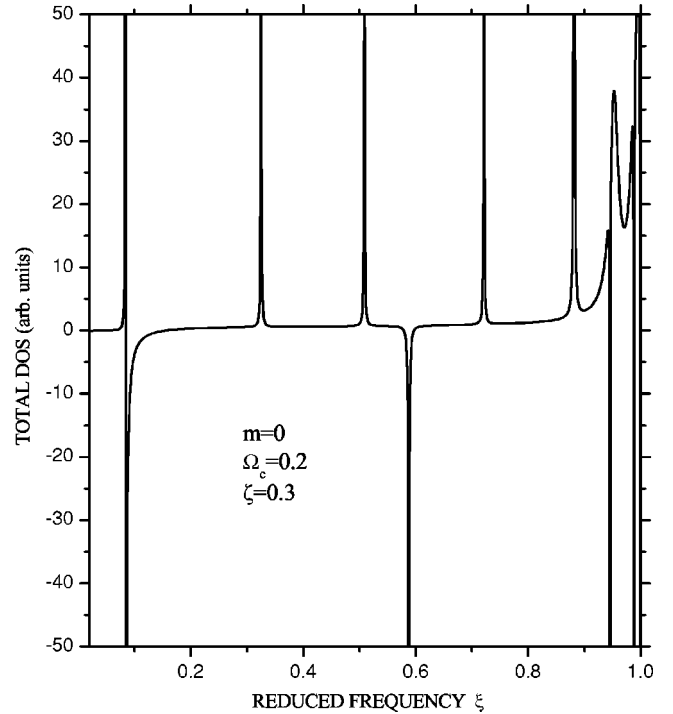

FIG. 9. Total density of states for $m=0$ and $\zeta=0.3$. The higher (lower) negative peak emerges from the first (second) perturbation and has no physical significance. The rest of the parameters used are the same as in Fig. 7.

0.5087, 0.7213, and 0.8819 corresponding to the interface R_1, whereas the interface R_2 captures only two low DOS peaks at $\xi=0.0835$ and 0.8819. That means that the two interfaces in the coaxial cylindrical geometry have different preferences. As it was pointed out before,[19] it seems that the two interfaces are more sensitive to the geometry and less sensitive to the materials in the bounding media. That is to say that the response of the two interfaces does not have to be identical simply because the bounding media are exactly the same. It is noteworthy that only the highest three peaks occurring at $\xi=0.8819$, 0.9541, and 0.9924 in the local DOS are shared by both interfaces. Moreover, except for the lowest one at the interface R_2, which corresponds to the confined plasmon mode, all of the higher resonances explain the radiative modes at this value of ζ.

Figure 9 presents the total density of states for the same system as studied in Figs. 7 and 8 for $m=0$ and $\zeta=0.3$. One can notice at once that there are five positive resonance peaks lying at the same frequencies as those in the local DOS (summing up all the peaks at both interfaces, but excluding the two highest ones). In addition, there are two negative peaks at $\xi=0.0854$ and 0.5878. We find that the lower (upper) negative peak comes from the second (first) perturbation alone where the Bessel function J_1 vanishes. That is to say that the position of the lower (upper) negative peak refers to the first (second) zero of J_1. Both positive peaks of the first perturbation, which were seen to correspond to the first two zeros of J_0, have disappeared in the total DOS. A careful look at the dispersion relations in Fig. 7 reveals that there is an excellent correspondence between the resonance peaks in the DOS and the magnetoplasmon dispersion for a given ζ,
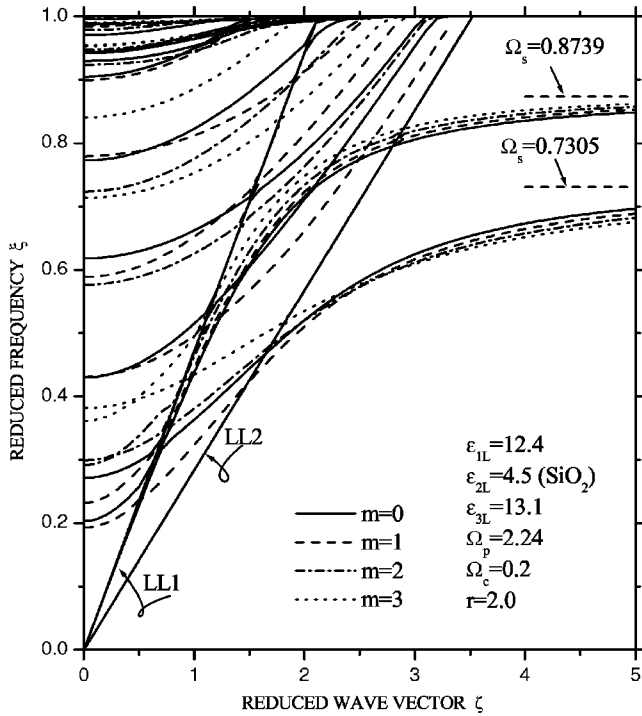
FIG. 10. Magnetoplasmon dispersion in a GaAs plasma (ϵ_{3L} =13.1) shell sandwiched between unidentical $Ga_{1-x}Al_xAs$ (ϵ_{1L} =12.4) and SiO_2 (ϵ_{2L}=4.5) dielectrics. The solid line labeled as $LL1$ ($LL2$) refers to the light line in the SiO_2 ($Ga_{1-x}Al_xAs$). The dashed horizontal line labeled as Ω_s=0.7305 (Ω_s=0.8739) is the asymptotic frequency for the interface R_1 (R_2). The parameters used are as listed in the picture.

except for the lowest extended mode in the radiative region (towards the left of the light line) that could be reproduced neither in the local nor in the total DOS. This is not surprising, however, given the complexity of searching the zeros of the determinant for the dispersion spectrum in Fig. 7. We did not pay much attention to the two highest positive as well as negative peaks (which come from the third perturbation alone) in the local and/or total DOS for the reason that there is, in general, not a very good correspondence between the dispersion spectrum and the DOS for the frequencies lying *above* a characteristic curve that corresponds to $\beta_\pm=0$ (i.e., at $\xi>0.9055$ at the origin). The disagreement is, of course, attributed to the strategy of determining the zeros of a complex function for the purpose of plotting the dispersion curves, for example.

Figure 10 illustrates the magnetoplasmon dispersion for the GaAs plasma shell bounded by unidentical dielectrics ($Ga_{1-x}Al_xAs$ in the inner cylinder and SiO_2 in the outer semi-infinite medium). For other parameters involved in the computation, we consider Ω_p=2.24, Ω_c=0.2, and r=2.0. The solid, dashed, dashed-dotted, and dotted curves represent, respectively, the case for m=0, 1, 2, and 3. The two solid straight lines marked as $LL1$ and $LL2$ refer to the light lines in the dielectric media SiO_2 and $Ga_{1-x}Al_xAs$, respectively. The two dashed horizontal lines labeled as Ω_s=0.7305 and Ω_s=0.8739 stand for the asymptotic frequencies for the plasmon-polaritons propagating at the interface R_1 and R_2, respectively. Unlike as in the symmetric case (see Fig. 7), the
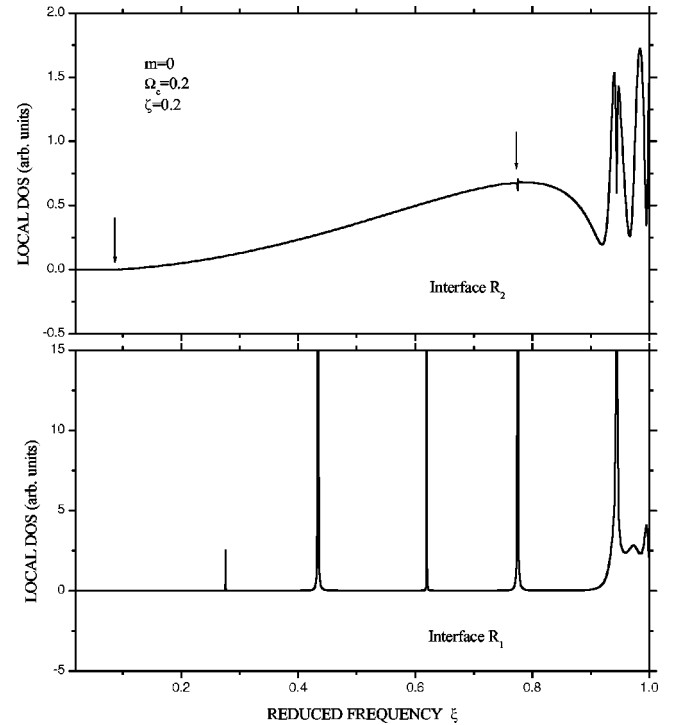

FIG. 11. Local density of states at the interface R_1 (R_2) in the lower (upper) panel for m=0 and ζ=0.2. We call attention to the smaller DOS resonances, indicated by the arrows, corresponding to the interface R_2. The rest of the parameters used are the same as in Fig. 10.

two magnetoplasma modes at large propagation vector ζ approach the different asymptotic limits. Comparing Fig. 10 with Fig. 7 reveals that the asymmetric case yields a relatively richer spectrum at least for the radiative modes for a given m. Interesting, but not unexpected, is the fact that only the lowest pair of modes for every m crosses the rightmost light line and attains the character of a pure magnetoplasmon-polariton before becoming asymptotic to the respective frequencies. The lower confined magnetoplasmons at $\zeta \simeq 2.5$ demonstrate the same kind of *focusing* effect for nonzero m as those observed, for example, in Figs. 5 and 7. At $\zeta \gtrsim 2.5$, the originally lower (higher) m mode becomes the higher (lower) frequency mode until at very large ζ, where they all become asymptotic to the lower limit (i.e., ξ =0.7305).

Figure 11 depicts the local density of states at interface R_1 (R_2) in the lower (upper) panel for m=0 and ζ=0.2. The other parameters are the same as those used in Fig. 10. We call attention to the point stated in the end of the discussion related to Fig. 9 and henceforth will not count any peak at $\xi>0.9055$ that refers to $\beta_\pm=0$ at ζ=0. We can see (first) four clear resonances lying at ξ=0.2758, 0.4339, 0.6199, and 0.7751 at interface R_1, whereas the interface R_2 we observe only two at ξ=0.0928 and 0.7752. Thus the two interfaces share only the highest resonance in the local DOS and with a difference of magnitude. Again, the two interfaces pose different preferences, and that really makes more sense here because of the asymmetric configuration. Note that only the lowest resonance at interface R_2 belongs to the confined plas-
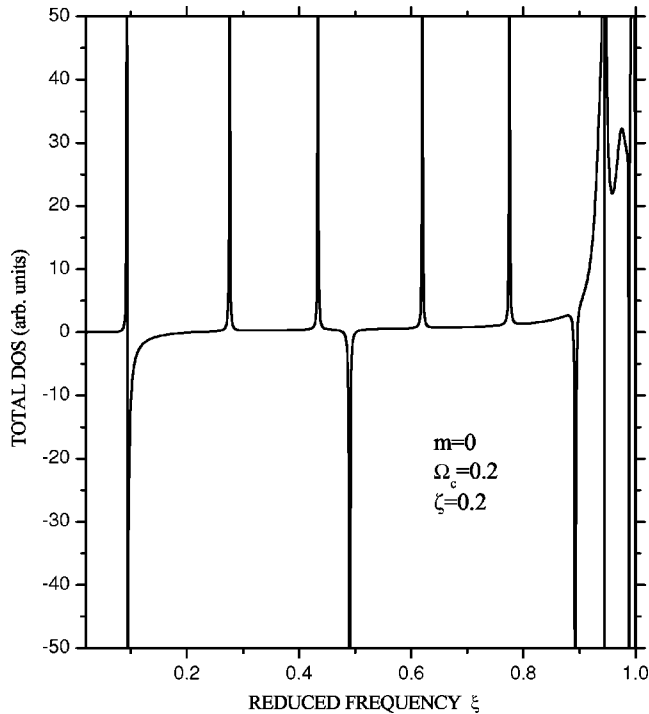
FIG. 12. Total density of states for $m=0$ and $\zeta=0.2$. The rest of the parameters used are the same as in Fig. 10. While the lowest negative peak emerges from the second perturbation, the two higher peaks come from the first perturbation. Such negative peaks have no physical significance.

FIG. 13. Plasmon dispersion in a $Ga_{1-x}Al_xAs$ dielectric ($\epsilon_{3L}=12.4$) shell sandwiched between identical GaAs plasmas ($\epsilon_{1L}=13.1=\epsilon_{2L}$). There are four groups of curves for four different values of m. The solid, straight line labeled as LL refers to the light line in the $Ga_{1-x}Al_xAs$ dielectric. The parameters used in the computation are as listed in the picture.

mon mode, while the rest of the higher ones correspond to the radiative modes. As regards the peaks at $\xi>0.9055$, although there is a reasonable consistency between the peaks at the two interfaces, we do not, for the moment, want to make any remark on the correspondence these peaks may or may not have with the respective modes in Fig. 10, for the reason stated before.

Figure 12 shows the total density of states for the same system as discussed in Figs. 10 and 11 for $m=0$, $\Omega_c=0.2$, and $\zeta=0.2$. We find that there are five well-defined positive resonances lying at the same frequencies as those specifying the resonance peaks in the local DOS (summing up all the peaks at both interfaces in Fig. 11). In addition, there are three negative peaks occurring at $\xi=0.0945$, 0.4899, and 0.8928, which have no physical significance. While the first one comes from the second perturbation, the pair of the second and third negative peaks emerges from the first perturbation (i.e., $|\tilde{g}_1^{-1}|=0$); their positions in frequency correspond to the first three zeros of the Bessel function J_1. The two positive resonances observed in the first perturbation, which correspond to the first two zeros of J_0, have disappeared from the total DOS. It is found that all five resonances in the DOS exactly reproduce the frequencies of the plasmon modes of Fig. 10 at the given ζ, with an exception for the lowest radiative mode above the light line $LL1$. However, this mode is found to have the same story as the corresponding one in Fig. 7, and hence our comments made in relation to Fig. 9 remain valid. Again, we did not count on the peaks emerging at $\xi>0.9055$ (see above), albeit we understand, for example, that the two negative peaks come from the third perturbation alone.
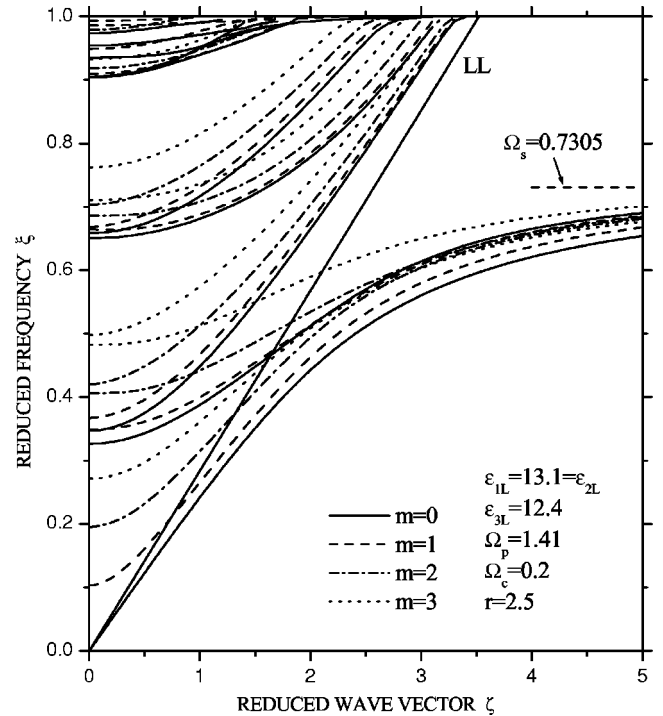
Finally, we take up the case of a dielectric ($Ga_{1-x}Al_xAs$) shell symmetrically bounded by two identical GaAs plasmas for $\Omega_p=1.41$, $\Omega_c=0.2$, and the aspect ratio $r=2.5$. The results for the magnetoplasmon dispersion in terms of the dimensionless frequency (ξ) and wave vector (ζ) are plotted in Fig. 13. The solid, dashed, dashed-dotted, and dotted curves correspond to $m=0$, 1, 2, and 3, respectively. The solid, straight line marked as LL refers to the light line in the dielectric shell, and the dashed horizontal line labeled as $\xi=0.7305$ indicates the asymptotic frequency for the magnetoplasmon-polariton at the large value of ζ, where nonretardation effects are negligible. One can easily notice that while the number of the modes in the nonradiative region is still two, the number of radiative modes (towards the left of the light line) is larger for any m as compared to that in Figs. 7 and 10. Also, it is evident that no such nasty mode (such as the lowest radiative mode encountered in Figs. 7 and 10) is seen to emerge in this case. In this case, the kind of *focusing* effect we discussed before occurs for the upper branch of the confined modes, is not so sharp, and is seen to shift to a higher value of $\zeta\simeq2.85$. The trend of getting the radiative magnetoplasma modes accumulated in the frequency range specified by $0.9055\lesssim\xi\lesssim1.0$ bears nearly the same story as in Figs. 7 and 10. This frequency range seems to be extremely sensitive as regards the search for the zeros of the kind of complex function we have had in such systems.

Figure 14 illustrates the local density of states at interface R_1 (R_2) in the lower (upper) panel for $m=0$, $\Omega_c=0.2$, and ζ
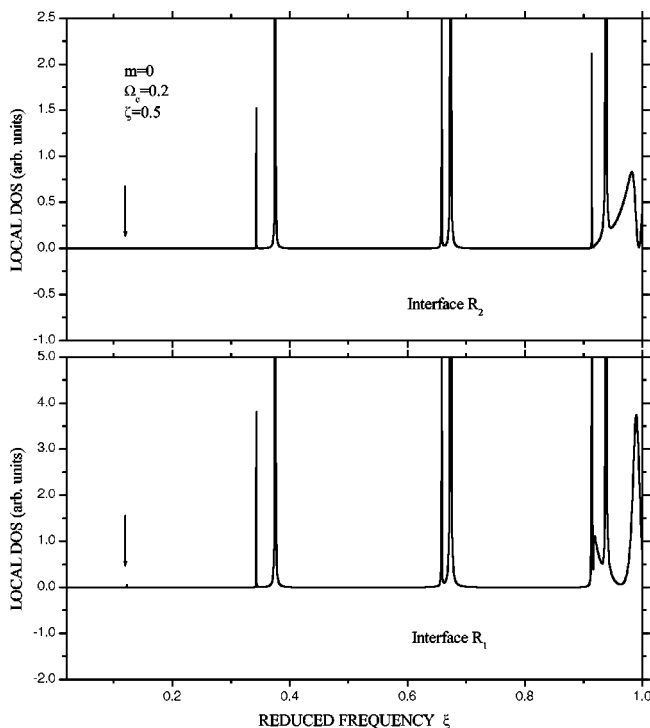
FIG. 14. Local density of states for $m=0$ and $\zeta=0.5$. The rest of the parameters used are the same as in Fig. 13. We call attention to the smaller (indiscernible) resonances at $\xi=0.1231$, indicated by the arrows.
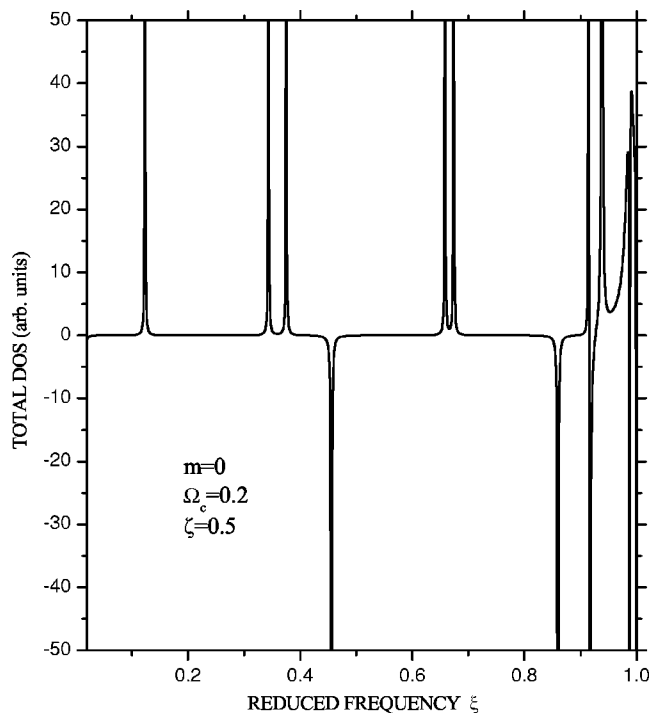

FIG. 15. Total density of states for $m=0$ and $\zeta=0.5$. The rest of the parameters used are the same as in Fig. 13. Both of the negative peaks emerge from the third perturbation alone and have no physical significance.
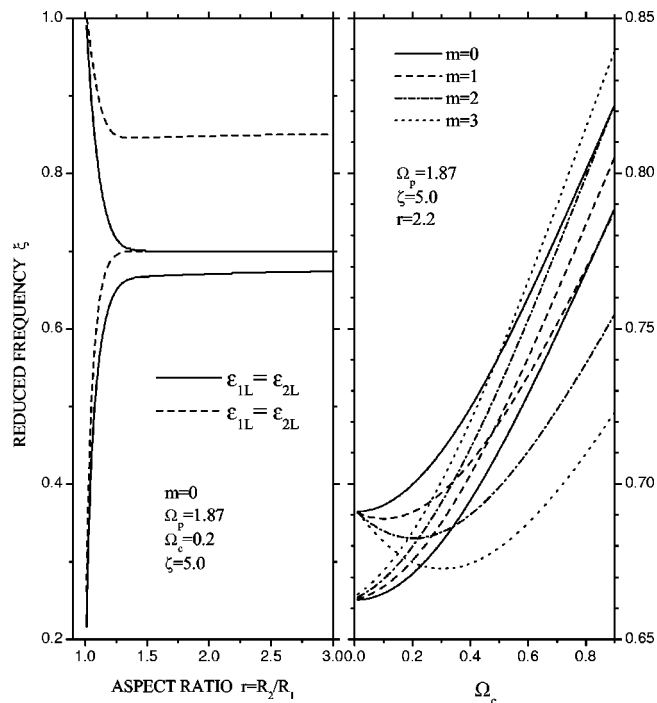

FIG. 16. The effect of the variation of the aspect ratio r $=R_2/R_1$ (left panel) and the magnetic field intensity (right panel) on the magnetoplasmon frequency for a given $\zeta=5.0$. The solid (dashed) lines refer to the geometry studied in Fig. 7 (Fig. 10). The rest of the parameters are listed in the picture.

$=0.5$. It is found that there are seven well-defined resonances lying at $\xi=0.1231$, 0.3434, 0.3751, 0.6582, 0.6737, 0.9142, and 0.9382, shared by both interfaces, of course, with a difference of magnitude. In that sense, this case is much different than the previous one of the plasma shell between two dielectrics (see, for example, Figs. 8 and 11). Again, it is only the lowest resonance that substantiates the confined plasmon mode below the light line; the rest correspond to the radiative modes for this value of ζ. Interestingly, the DOS resonances are sharper in this case even within the delicate frequency regime (i.e., $0.9055 \lesssim \xi \lesssim 1.0$). We do not count on the highest jump occurring at the frequency $\xi \approx 0.98$.

Figure 15 shows the total density of states for the same system as represented by Figs. 13 and 14 for $m=0$, $\Omega_c=0.2$, and $\zeta=0.5$. We observe that there are seven well-defined positive resonances located at the same frequencies as those specifying the similar resonance peaks in the local DOS in Fig. 14. Moreover, there are two negative resonances that are seen to emerge at $\xi=0.4557$ and 0.8598. These negative peaks are a consequence of the third perturbation alone that produces three positive peaks lying at $\xi=0.1420 \Rightarrow \beta_3=0$, 0.4398, and 0.8507 and the two negative peaks as mentioned above. While all three positive peaks disappear from the total DOS, the two negative peaks survive. All the (positive plus negative) peaks in the third perturbation are seen to be the exact solutions of $|\tilde{g}_3^{-1}|=0$. The case studied in Figs. 13–15 for the coaxial cylindrical geometry seems to be the clearest one where there is no conflict at all between the DOS resonances and the plasmon dispersion. However, this remark is reserved with respect to this notoriously delicate frequency region $(0.9055 \lesssim \xi \lesssim 1.0)$.

Figure 16 illustrates the effect of the variation of aspect ratio r (left panel) and the magnetic field Ω_c (right panel) on the frequency of the magnetoplasmons of a system made up of a plasma shell bounded by two identical or unidentical dielectrics. The solid (dashed) lines in the left panel correspond to the case in which the bounding media are identical (unidentical). The plot in the left panel clearly reveals that the magnetoplasmon frequencies at higher ζ (where the retardation effect becomes very small) intend to be sharply varying for a very thin shell, but start becoming (almost) insensitive at the larger values of r. (See, for example, the behavior at $r \geqslant 1.5$.) The right panel demonstrates that while the frequency of the lower mode of the system (for all values of m) increases monotonously with the magnetic field, the upper mode does reveal an opposite behavior, at least for smaller B. The latter behavior of the upper mode is seen to be sharper for a larger value of integer m. One can also notice that for certain values of B, both (nonzero) m modes cross each other and the higher the m, the smaller the value of that B. We hope that the variation of the aspect ratio r should have a similar effect on the plasmon or magnetoplasmon frequencies in other *curved* plasmas, as depicted in the left panel in Fig. 16.

C. Some specific remarks

It is noteworthy that all the negative peaks showing up in the variation of the total DOS, for example, in Figs. 6, 9, 12, and 15, originate from the initial systems (or the so-called initial perturbations) comprising the resultant system. As noticed before, these are seen to be obtainable from the zeros of $|\tilde{g}_i^{-1}|$ (with $i \equiv 1$, 2, or 3) wherever a dielectric medium is bounded by one (in the case of a single-interface system) or two (in the case of a double-interface system) black boxes. Since the black box does not represent a true physical system, though it is an essential ingredient of the theoretical scheme,[13] these peaks have, in fact, no physical significance. However, they do exist with a negative sign in the total DOS, independently of the size, shape, and dimensionality of the system concerned.

Notice that most of the modes covered by our results on the DOS correspond to those that fall in the radiative regime (i.e., towards the left of the left-most light line in, for example, Figs. 5, 7, 10, and 13). The LDOS in Figs. 6, 8, and 11 indicate that these modes are actually those of the $Ga_{1-x}Al_xAs$ dielectric bounded by the GaAs plasma, confined on the dielectric side and forbidden from propagating in the GaAs plasma. This is true despite the fact that depending on the aspect ratio r the radiative modes in Figs. 8 and 11 can interact with the surrounding dielectric in the outer medium and hence may differ slightly from those in Fig. 6. Similarly, the modes in Fig. 14 are essentially those of the $Ga_{1-x}Al_xAs$ shell that are disallowed to propagate in the neighboring plasmas. This also explains why such peaks are so strong. The modes in the nonradiative regime tend to bear a different story. They originate from the dielectric-plasma heterointerface(s) and are truly magnetoplasmon-polariton-like.

It is not a *part and parcel* of the work presented in this paper, but we think it is worthwhile to add a word of warning about a very subtle issue regarding the delusive traces of the edge magnetoplasmons (EMPs). We now know that the EMPs—which are by definition the 2D analogs of the 3D surface plasmons and are characterized by their frequencies decreasing with increasing magnetic field[1]—have their existence known in several kinds of geometries, such as disks and rings. So it occurred to us that if we take the propagation vector $\zeta = 0$ and compute the magnetoplasmon frequency as a function of magnetic field B (or Ω_c) for, for example, a very thin plasma shell sandwiched between two identical or unidentical dielectrics, we must obtain something that would mimic these EMPs. To our surprise, this is exactly what turned out until and unless we tried to understand what these modes actually were. For $\zeta = 0$ and $r = 1.05$, we found that, apart from such minutely distorted radiative modes, there is a just one such mode that starts from the plasma frequency (i.e., $\xi = 1$) the frequency of which gradually decreases with increasing B. Furthermore, if we increase r, the number of such modes starts increasing. So this spectrum looks just like the one for the EMPs. However, we found that for a very thin plasma shell (i.e., $r \rightarrow 0$) such a mode is nothing but the solution of $\beta_\pm = 0$, and for a thick plasma shell (say, $r = 2.2$), while the lowest one remains intact (and explicable as the solution of $\beta_\pm = 0$), the higher modes could not be substantiated by the local and/or total DOS. This led us to infer that such a spectrum is nothing but the delusive traces of the EMPs.

V. CONCLUDING REMARKS

In conclusion, we investigated the magnetoplasmon dispersion and the density of states in the coaxial cylindrical geometries in the presence of an applied axial magnetic field. We derived the general dispersion relations using a Green-function theory in the framework of IRT,[13] which has now found widespread use in studying the numerous excitations in various composite systems.[15–19] In doing so, we not only clarified some basic notions in the use of cylindrical geometries, but also diagnosed our general analytical results under special limits to reproduce some well-known results on planar systems, both with and without applied magnetic fields. We also successfully attempted to substantiate our results on plasmon dispersion through the computation of the local and total density of states. While we considered the effect of retardation, the absorption was neglected throughout, except for a small imaginary part added to the frequencies for the purpose of computing the DOS. We hope that the present methodology for coaxial cylindrical geometries proves to be a powerful theoretical framework for studying, for example, the intrasubband plasmons and magnetoplasmons in multi-walled carbon nanotubes.

The experimental observation of radiative as well as nonradiative magnetoplasmon modes in such coaxial, cylindrical geometries would be of great interest. Such experiments could possibly involve the well-known attenuated total reflection, the scattering of high-energy electrons, or even resonant Raman spectroscopy. Electron-energy-loss spectroscopy (EELS) is already becoming known as a powerful technique

for studying the electronic structure, dielectric properties, and plasmon excitations in carbon nanotubes and carbon onions, for example. Our preference for plotting the numerical results in terms of the dimensionless frequency and propagation vector leaves free an option of choosing a lower or higher plasma frequency, just as for the aspect ratio.

Many important problems remain open in the context of the present investigation. The issues that need to be considered and could give better insight into the problem include the role of absorption, the effects of the spatial dispersion, the plasmons coupling to the optical phonons, effect of an applied electric field that may create the drifted charge carriers and help study the instability mechanism, and the making of a multicoaxial waveguide system that employs, for example, left-handed materials, to name a few. Currently, we have been investigating the plasma effects in such multicoaxial waveguide systems that exploit the materials characterized by *negative* permittivity and permeability and the results will be reported shortly.

APPENDIX A: LOCAL DIELECTRIC FUNCTIONS

The dielectric tensor components employed in this work are defined as follows:

$$\epsilon_{xx} = \epsilon_{yy} = \epsilon_L \left\{ 1 - \frac{\omega_p^2(\omega + i\nu)}{\omega[(\omega + i\nu)^2 - \omega_c^2]} \right\}, \qquad (A1)$$

$$\epsilon_{yx} = -\epsilon_{xy} = -i\epsilon_L \frac{\omega_p^2 \omega_c}{\omega[(\omega + i\nu)^2 - \omega_c^2]}, \qquad (A2)$$

$$\epsilon_{zz} = \epsilon_L \left[1 - \frac{\omega_p^2}{\omega(\omega + i\nu)} \right], \qquad (A3)$$

where ϵ_L is the background dielectric constant, ν is the free-carrier-collision frequency, ω_p is the screened-plasma frequency, and ω_c is the electron-cyclotron frequency.

If we also consider the effect of phonons, which, in a way, incorporates the coupling of the plasmons (or magnetoplasmons) to the optical phonons, then the background dielectric constant ϵ_L has to be replaced by its frequency dependent expression,

$$\epsilon_L(\omega) = \epsilon_\infty \left[\frac{\omega_{LO}^2 - \omega^2 - i\Gamma\omega}{\omega_{TO}^2 - \omega^2 - i\Gamma\omega} \right], \qquad (A4)$$

where ϵ_∞ is the high-frequency dielectric constant, Γ is the optical-phonon damping frequency, and ω_{LO} and ω_{TO} are, respectively, the longitudinal and transverse optical-phonon frequencies at the zone center of the Brillouin zone. Remember that the convention of an additional subscript j over all quantities applies. This subscript specifies the perturbation concerned.

APPENDIX B: SEVERAL IDENTITIES RELATING x_i, γ_i, β_i, P_i, AND M

Here we enlist some identities interrelating x_i, γ_i, β_i, P_i, and M_i, which have proved to be extremely useful in simplifying otherwise quite involved mathematical steps, particularly those concerned with the matrix elements of, say, $\widetilde{A}_j$, $\widetilde{\Delta}_j$, $\widetilde{G}_j^{-1}$, and $\widetilde{g}_j^{-1}$. The first category of identities is $\gamma_{j3}^4 = M_j \gamma_{j1}^2 \gamma_{j2}^2$, $S_{j1}S_{j3} = S_{j5}S_{j6}$, $S_{j1}S_{j4} = S_{j5}S_{j7}$, $S_{j2}S_{j6} = x_{j1}x_{j2}S_{j7}$, $S_{j3}S_{j7} = S_{j2}$, $S_{j4}S_{j6} = S_{j2}$, $S_{j2} = x_{j1}x_{j2}\gamma_{j0}S_{j8}$, $S_{j3}S_{j8} = S_{j4}/\gamma_{j0}$, where $M_j = (1 + x_{j1}x_{j2})$ and $\gamma_{j0} = \gamma_{j1}^4/(q_0^4\epsilon_{j2}^2)$. The second category of identities associated with A_i, B_i, C_i, and D_i is

$$A_1 D_1 + x_1 x_2 B_1 C_1 = 0, \qquad (B1)$$

$$A_2 D_2 + x_1 x_2 B_2 C_2 = 0, \qquad (B2)$$

$$A_1 D_2 + A_2 D_1 = \frac{1}{M^2 S^2} [(\beta_1^4 + \beta_2^4)M - 2\beta_1^2\beta_2^2], \qquad (B3)$$

$$B_1 C_2 + B_2 C_1 = -\frac{2}{M^2 S^2}\beta_1^2\beta_2^2, \qquad (B4)$$

$$[(A_1 D_2 + A_2 D_1) + x_1 x_2 (B_1 C_2 + B_2 C_1)] = \frac{1}{M}, \qquad (B5)$$

…, etc. The third category of internal identities is

$$P_1 + P_2 = (\beta_1^2 + \beta_2^2)M, \qquad P_1 P_2 = \beta_1^2\beta_2^2 M, \qquad (B6)$$

$$\begin{aligned}
(P_1 - \beta_1^2 M)\beta_1^2 - P_2(P_1 - \beta_1^2) &= 0, \\
(P_1 - \beta_2^2 M)\beta_1^2 - P_2(P_1 - \beta_1^2) &= MS\beta_1^2, \\
(P_1 - \beta_1^2 M)\beta_2^2 - P_2(P_1 - \beta_2^2) &= -MS\beta_2^2, \\
(P_1 - \beta_2^2 M)\beta_2^2 - P_2(P_1 - \beta_2^2) &= 0
\end{aligned} \qquad (B7)$$

$$\begin{aligned}
(P_2 - \beta_1^2 M)(P_1 - \beta_2^2) + x_1 x_2 P_1 \beta_2^2 &= -MS(P_1 - \beta_2^2), \\
(P_2 - \beta_1^2 M)(P_1 - \beta_1^2) + x_1 x_2 P_1 \beta_1^2 &= 0, \\
(P_2 - \beta_2^2 M)(P_1 - \beta_2^2) + x_1 x_2 P_1 \beta_2^2 &= 0, \\
(P_2 - \beta_2^2 M)(P_1 - \beta_1^2) + x_1 x_2 P_1 \beta_1^2 &= MS(P_1 - \beta_1^2),
\end{aligned} \qquad (B8)$$

$$\begin{aligned}
(P_1 - \beta_1^2)(P_2 - \beta_2^2) + x_1 x_2 \beta_1^2\beta_2^2 &= S(P_1 - \beta_1^2 M), \\
(P_1 - \beta_2^2)(P_2 - \beta_1^2) + x_1 x_2 \beta_1^2\beta_2^2 &= -S(P_1 - \beta_2^2 M).
\end{aligned} \qquad (B9)$$

Similar other identities follow if we just interchange P_1 and P_2. Remember that we have not specified the subscript j in

Eqs. (B1)–(B4) for brevity, which has to be used on all quantities while referring to a specific perturbation. The third category of identities quite often used here involves some well-known relations between the Bessel functions. It is

$$\zeta'_\nu(z) = -\zeta_{\nu+1}(z) + \frac{\nu}{z}\zeta_\nu(z), \tag{B10}$$

where $\zeta \equiv J$, Y, or H, which are, respectively, the Bessel functions of the first, second, and third kinds. z refers to the complex argument and ν to the integer order thereof. The prime stands for the derivative of the respective function with respect to the argument. The other most useful identity is

$$H_\nu(z)J_\nu(z)\left[\frac{H'_\nu(z)}{H_\nu(z)} - \frac{J'_\nu(z)}{J_\nu(z)}\right] = \frac{2i}{\pi z}. \tag{B11}$$

The asymptotic expansions for the large arguments (i.e., $|z| \to \infty$) of these Bessel functions are specified by

$$J_\nu(z) \cong \sqrt{\frac{2}{\pi z}}\cos\left[z - \frac{1}{2}\left(\nu + \frac{1}{2}\right)\pi\right],$$

$$Y_\nu(z) \cong \sqrt{\frac{2}{\pi z}}\sin\left[z - \frac{1}{2}\left(\nu + \frac{1}{2}\right)\pi\right], \tag{B12}$$

$$H_\nu(z) \cong \sqrt{\frac{2}{\pi z}}\exp\left\{i\left[z - \frac{1}{2}\left(\nu + \frac{1}{2}\right)\pi\right]\right\}.$$

As such, we obtain

$$\frac{J'_\nu(z)}{J_\nu(z)} = -i, \quad \frac{H'_\nu(z)}{H_\nu(z)} = +i. \tag{B13}$$

APPENDIX C: DETAILS FOR SEC. III B ON THE FIRST PERTURBATION

First of all, it should be pointed out that we will not use the additional subscript j (which means $j=1$ in the present case) with other quantities, except for S_{ji}, for the sake of brevity. However, the convention of using this additional subscript over all quantities applies. The matrix elements in Eq. (3.6) are defined as

$$G_1(11) = -\frac{1}{S_{11}}[A_1 H_m(\beta_1\rho)J_m(\beta_1\rho') + A_2 H_m(\beta_2\rho)J_m(\beta_2\rho')], \tag{C1}$$

$$G_1(21) = \frac{S_{13}}{S_{15}}[B_1 H_m(\beta_1\rho)J_m(\beta_1\rho') + B_2 H_m(\beta_2\rho)J_m(\beta_2\rho')], \tag{C2}$$

$$G_1(12) = -\frac{S_{16}}{S_{11}}[C_1 H_m(\beta_1\rho)J_m(\beta_1\rho') + C_2 H_m(\beta_2\rho)J_m(\beta_2\rho')], \tag{C3}$$

$$G_1(22) = -\frac{1}{S_{15}}[D_1 H_m(\beta_1\rho)J_m(\beta_1\rho') + D_2 H_m(\beta_2\rho)J_m(\beta_2\rho')]. \tag{C4}$$

The matrix elements in Eq. (3.7) are defined as

$$A_1(11) = \{-[(P_2 - \beta_1^2) - x_1 x_2 \beta_1^2]z_1 H'_m(z_1)J_m(z_1) + [(P_2 - \beta_2^2) - x_1 x_2 \beta_2^2]z_2 H'_m(z_2)J_m(z_2) + S_{12}P_2 H_m(z_1)J_m(z_1) - S_{12}P_2 H_m(z_2)J_m(z_2)\}, \tag{C5}$$

$$A_1(21) = \{+x_1 P_2 z_1 H'_m(z_1)J_m(z_1) - x_1 P_2 z_2 H'_m(z_2)J_m(z_2) + S_{14}[(P_2 - \beta_1^2) - \gamma_0^{-1}\beta_1^2]H_m(z_1)J_m(z_1) - S_{14}[(P_2 - \beta_2^2) - \gamma_0^{-1}\beta_2^2]H_m(z_2)J_m(z_2)\}, \tag{C6}$$

$$A_1(12) = \{-x_2 P_1 z_1 H'_m(z_1)J_m(z_1) + x_2 P_1 z_2 H'_m(z_2)J_m(z_2) - S_{17}[(P_1 - \beta_1^2) - x_1 x_2 \beta_1^2]H_m(z_1)J_m(z_1) + S_{17}[(P_1 - \beta_2^2) - x_1 x_2 \beta_2^2]H_m(z_2)J_m(z_2)\}, \tag{C7}$$

$$A_1(22) = \{-[(P_1 - \beta_1^2) - x_1 x_2 \beta_1^2]z_1 H'_m(z_1)J_m(z_1) + [(P_1 - \beta_2^2) - x_1 x_2 \beta_2^2]z_2 H'_m(z_2)J_m(z_2) + S_{18}[(P_1 - \beta_1^2) + x_1 x_2 \gamma_0 \beta_1^2]H_m(z_1)J_m(z_1) - S_{18}[(P_1 - \beta_2^2) + x_1 x_2 \gamma_0 \beta_2^2]H_m(z_2)J_m(z_2)\}, \tag{C8}$$

where $z_1 = \beta_1 R_1$ and $z_2 = \beta_2 R_1$. The prime on the Bessel functions stands for the derivative of the respective quantity with respect to the full argument. The matrix elements in Eq. (3.8) are defined as

$$\Delta_1(11) = A_1(11) \quad \text{with } H'_m J_m \text{ replaced by } J'_m H_m, \tag{C9}$$

$$\Delta_1(21) = A_1(21) \quad \text{with } H'_m J_m \text{ replaced by } J'_m H_m, \tag{C10}$$

$$\Delta_1(12) = A_1(12) \quad \text{with } H'_m J_m \text{ replaced by } J'_m H_m, \tag{C11}$$

$$\Delta_1(22) = A_1(22) \quad \text{with } H'_m J_m \text{ replaced by } J'_m H_m. \tag{C12}$$

The matrix elements in Eq. (3.11) are defined as

$$h_1(11) = -\frac{1}{S_{15}}\{[-(P_1 - \beta_1^2)z_2 J_m(z_1)J'_m(z_2) + (P_1 - \beta_2^2)z_1 \times J'_m(z_1)J_m(z_2)]H_m(z_1)H_m(z_2) - S_{12} \times (\beta_1^2 - \beta_2^2)J_m(z_1)H_m(z_1)J_m(z_2)H_m(z_2)\}, \tag{C13}$$

$$h_1(21) = \frac{1}{S_{15}}\{[x_1\beta_1^2 z_2 J_m(z_1)J'_m(z_2) - x_1\beta_2^2 z_1 J'_m(z_1)J_m(z_2)] \times H_m(z_1)H_m(z_2) + S_{14}(\beta_1^2 - \beta_2^2) \times J_m(z_1)H_m(z_1)J_m(z_2)H_m(z_2)\}, \tag{C14}$$

$$h_1(12) = -\frac{1}{S_{11}}\{[x_2\beta_1^2 z_2 J_m(z_1)J'_m(z_2) - x_2\beta_2^2 z_1 J'_m(z_1)J_m(z_2)]$$
$$\times H_m(z_1)H_m(z_2) + S_{17}(\beta_1^2 - \beta_2^2)$$
$$\times J_m(z_1)H_m(z_1)J_m(z_2)H_m(z_2)\}, \quad \text{(C15)}$$

$$h_1(22) = \frac{1}{S_{11}}\{[(P_2 - \beta_1^2)z_2 J_m(z_1)J'_m(z_2) - (P_2 - \beta_2^2)z_1$$
$$\times J'_m(z_1)J_m(z_2)]H_m(z_1)H_m(z_2) - S_{18}$$
$$\times (\beta_1^2 - \beta_2^2)J_m(z_1)H_m(z_1)J_m(z_2)H_m(z_2)\}. \quad \text{(C16)}$$

APPENDIX D: DETAILS FOR SEC. III C ON THE SECOND PERTURBATION

Again, it should be pointed out that we will not use this additional subscript j (which means $j=2$ in the present case) with other quantities, except for S_{ji}, for the sake of brevity. However, the convention of using this additional subscript over all quantities applies. The matrix elements in Eq. (3.14) are defined as

$$G_2(11) = -\frac{1}{S_{21}}[A_1 J_m(\beta_1\rho)H_m(\beta_1\rho') + A_2 J_m(\beta_2\rho)H_m(\beta_2\rho')],$$
$$\text{(D1)}$$

$$G_2(21) = \frac{S_{23}}{S_{25}}[B_1 J_m(\beta_1\rho)H_m(\beta_1\rho') + B_2 J_m(\beta_2\rho)H_m(\beta_2\rho')],$$
$$\text{(D2)}$$

$$G_2(12) = -\frac{S_{26}}{S_{21}}[C_1 J_m(\beta_1\rho)H_m(\beta_1\rho') + C_2 J_m(\beta_2\rho)H_m(\beta_2\rho')],$$
$$\text{(D3)}$$

$$G_2(22) = -\frac{1}{S_{25}}[D_1 J_m(\beta_1\rho)H_m(\beta_1\rho') + D_2 J_m(\beta_2\rho)H_m(\beta_2\rho')].$$
$$\text{(D4)}$$

The matrix elements in Eq. (3.15) are defined as

$$A_2(11) = \{-[(P_2 - \beta_1^2) - x_1 x_2\beta_1^2]z_1 J'_m(z_1)H_m(z_1) + [(P_2 - \beta_2^2)$$
$$- x_1 x_2\beta_2^2]z_2 J'_m(z_2)H_m(z_2) + S_{22}P_2 J_m(z_1)H_m(z_1)$$
$$- S_{22}P_2 J_m(z_2)H_m(z_2)\}, \quad \text{(D5)}$$

$$A_2(21) = \{+ x_1 P_2 z_1 J'_m(z_1)H_m(z_1) - x_1 P_2 z_2 J'_m(z_2)H_m(z_2)$$
$$+ S_{24}[(P_2 - \beta_1^2) - \gamma_0^{-1}\beta_1^2]J_m(z_1)H_m(z_1)$$
$$- S_{24}[(P_2 - \beta_2^2) - \gamma_0^{-1}\beta_2^2]J_m(z_2)H_m(z_2)\}, \quad \text{(D6)}$$

$$A_2(12) = \{- x_2 P_1 z_1 J'_m(z_1)H_m(z_1) + x_2 P_1 z_2 J'_m(z_2)H_m(z_2)$$
$$- S_{27}[(P_1 - \beta_1^2) - x_1 x_2\beta_1^2]J_m(z_1)H_m(z_1)$$
$$+ S_{27}[(P_1 - \beta_2^2) - x_1 x_2\beta_2^2]J_m(z_2)H_m(z_2)\}, \quad \text{(D7)}$$

$$A_2(22) = \{-[(P_1 - \beta_1^2) - x_1 x_2\beta_1^2]z_1 J'_m(z_1)H_m(z_1) + [(P_1 - \beta_2^2)$$
$$- x_1 x_2\beta_2^2]z_2 J'_m(z_2)H_m(z_2) + S_{28}[(P_1 - \beta_1^2)$$
$$+ \gamma_0 x_1 x_2\beta_1^2]J_m(z_1)H_m(z_1) - S_{28}[(P_1 - \beta_2^2)$$
$$+ \gamma_0 x_1 x_2\beta_2^2]J_m(z_2)H_m(z_2)\}, \quad \text{(D8)}$$

where $z_1 = \beta_1 R_2$ and $z_2 = \beta_2 R_2$. The prime on the Bessel functions stands for the derivative of the respective quantity with respect to the full argument. The matrix elements in Eq. (3.16) are defined as

$$\Delta_2(11) = A_2(11), \quad \text{with } J'_m H_m \text{ replaced by } H'_m J_m,$$
$$\text{(D9)}$$

$$\Delta_2(21) = A_2(21), \quad \text{with } J'_m H_m \text{ replaced by } H'_m J_m,$$
$$\text{(D10)}$$

$$\Delta_2(12) = A_2(12), \quad \text{with } J'_m H_m \text{ replaced by } H'_m J_m,$$
$$\text{(D11)}$$

$$\Delta_2(22) = A_2(22), \quad \text{with } J'_m H_m \text{ replaced by } H'_m J_m.$$
$$\text{(D12)}$$

The matrix elements in Eq. (3.19) are defined as

$$h_2(11) = -\frac{1}{S_{25}}\{[-(P_1 - \beta_1^2)z_2 H_m(z_1)H'_m(z_2) + (P_1 - \beta_2^2)z_1$$
$$\times H'_m(z_1)H_m(z_2)]J_m(z_1)J_m(z_2) - S_{22}$$
$$\times (\beta_1^2 - \beta_2^2)J_m(z_1)H_m(z_1)J_m(z_2)H_m(z_2)\}, \quad \text{(D13)}$$

$$h_2(21) = \frac{1}{S_{25}}\{[x_1\beta_1^2 z_2 H_m(z_1)H'_m(z_2) - x_1\beta_2^2 z_1 H'_m(z_1)H_m(z_2)]$$
$$\times J_m(z_1)J_m(z_2) + S_{24}(\beta_1^2 - \beta_2^2)$$
$$\times J_m(z_1)H_m(z_1)J_m(z_2)H_m(z_2)\}, \quad \text{(D14)}$$

$$h_2(12) = -\frac{1}{S_{21}}\{[x_2\beta_1^2 z_2 H_m(z_1)H'_m(z_2) - x_2\beta_2^2 z_1 H'_m(z_1)H_m(z_2)]$$
$$\times J_m(z_1)J_m(z_2) + S_{27}(\beta_1^2 - \beta_2^2)$$
$$\times J_m(z_1)H_m(z_1)J_m(z_2)H_m(z_2)\}, \quad \text{(D15)}$$

$$h_2(22) = \frac{1}{S_{21}}\{[(P_2 - \beta_1^2)z_2 H_m(z_1)H'_m(z_2) - (P_2 - \beta_2^2)z_1$$
$$\times H'_m(z_1)H_m(z_2)]J_m(z_1)J_m(z_2) - S_{28}$$
$$\times (\beta_1^2 - \beta_2^2)J_m(z_1)H_m(z_1)J_m(z_2)H_m(z_2)\}. \quad \text{(D16)}$$

APPENDIX E: DETAILS FOR SEC. III D ON THE THIRD PERTURBATION

Again, it should be pointed out that we will not use this additional subscript j (which means $j=3$ in the present case) over other quantities, except for S_{ji}, for the sake of brevity.

However, the convention of using this additional subscript over all quantities applies. The matrix elements in Eq. (3.22) are given as hereunder:

$$G_3(11) = -\frac{1}{S_{31}}[A_1 J_m(\beta_1\rho)H_m(\beta_1\rho') + A_2 J_m(\beta_2\rho)H_m(\beta_2\rho')],$$

(E1)

$$G_3(21) = \frac{S_{33}}{S_{35}}[B_1 J_m(\beta_1\rho)H_m(\beta_1\rho') + B_2 J_m(\beta_2\rho)H_m(\beta_2\rho')],$$

(E2)

$$G_3(31) = -\frac{1}{S_{31}}[A_1 H_m(\beta_1\rho)J_m(\beta_1\rho') + A_2 H_m(\beta_2\rho)J_m(\beta_2\rho')],$$

(E3)

$$G_3(41) = \frac{S_{33}}{S_{35}}[B_1 H_m(\beta_1\rho)J_m(\beta_1\rho') + B_2 H_m(\beta_2\rho)J_m(\beta_2\rho')],$$

(E4)

$$G_3(12) = -\frac{S_{36}}{S_{31}}[C_1 J_m(\beta_1\rho)H_m(\beta_1\rho') + C_2 J_m(\beta_2\rho)H_m(\beta_2\rho')],$$

(E5)

$$G_3(22) = -\frac{1}{S_{35}}[D_1 J_m(\beta_1\rho)H_m(\beta_1\rho') + D_2 J_m(\beta_2\rho)H_m(\beta_2\rho')],$$

(E6)

$$G_3(32) = -\frac{S_{36}}{S_{31}}[C_1 H_m(\beta_1\rho)J_m(\beta_1\rho') + C_2 H_m(\beta_2\rho)J_m(\beta_2\rho')],$$

(E7)

$$G_3(42) = -\frac{1}{S_{35}}[D_1 H_m(\beta_1\rho)J_m(\beta_1\rho') + D_2 H_m(\beta_2\rho)J_m(\beta_2\rho')],$$

(E8)

$$G_3(13) = -\frac{1}{S_{31}}[A_1 J_m(\beta_1\rho)H_m(\beta_1\rho') + A_2 J_m(\beta_2\rho)H_m(\beta_2\rho')],$$

(E9)

$$G_3(23) = \frac{S_{33}}{S_{35}}[B_1 J_m(\beta_1\rho)H_m(\beta_1\rho') + B_2 J_m(\beta_2\rho)H_m(\beta_2\rho')],$$

(E10)

$$G_3(33) = -\frac{1}{S_{31}}[A_1 H_m(\beta_1\rho)J_m(\beta_1\rho') + A_2 H_m(\beta_2\rho)J_m(\beta_2\rho')],$$

(E11)

$$G_3(43) = \frac{S_{33}}{S_{35}}[B_1 H_m(\beta_1\rho)J_m(\beta_1\rho') + B_2 H_m(\beta_2\rho)J_m(\beta_2\rho')],$$

(E12)

$$G_3(14) = -\frac{S_{36}}{S_{31}}[C_1 J_m(\beta_1\rho)H_m(\beta_1\rho') + C_2 J_m(\beta_2\rho)H_m(\beta_2\rho')],$$

(E13)

$$G_3(24) = -\frac{1}{S_{35}}[D_1 J_m(\beta_1\rho)H_m(\beta_1\rho') + D_2 J_m(\beta_2\rho)H_m(\beta_2\rho')],$$

(E14)

$$G_3(34) = -\frac{S_{36}}{S_{31}}[C_1 H_m(\beta_1\rho)J_m(\beta_1\rho') + C_2 H_m(\beta_2\rho)J_m(\beta_2\rho')],$$

(E15)

$$G_3(44) = -\frac{1}{S_{35}}[D_1 H_m(\beta_1\rho)J_m(\beta_1\rho') + D_2 H_m(\beta_2\rho)J_m(\beta_2\rho')].$$

(E16)

We would like to stress that the interface space M_s will be referred to as $(\rho=R_1,\rho'=R_1)$, $(\rho=R_1,\rho'=R_2)$, $(\rho=R_2,\rho'=R_2)$, and $(\rho=R_2,\rho'=R_1)$, respectively, in the first, second, third, and fourth quadrants made up of 2×2 submatrices, starting clockwise from the top-left quadrant. The matrix elements in Eq. (3.23) are defined as

$$\begin{aligned}A_3(11) = &\{[(P_2 - \beta_1^2) - x_1 x_2\beta_1^2]z_1 J_m'(z_1)H_m(z_1) - [(P_2 - \beta_2^2)\\ &- x_1 x_2\beta_2^2]z_2 J_m'(z_2)H_m(z_2) - S_{32}P_2 J_m(z_1)H_m(z_1)\\ &+ S_{32}P_2 J_m(z_2)H_m(z_2)\},\end{aligned}$$

(E17)

$$\begin{aligned}A_3(21) = &\{-x_1 P_2 z_1 J_m'(z_1)H_m(z_1) + x_1 P_2 z_2 J_m'(z_2)H_m(z_2)\\ &- S_{34}[(P_2 - \beta_1^2) - \gamma_0^{-1}\beta_1^2]J_m(z_1)H_m(z_1)\\ &+ S_{34}[(P_2 - \beta_2^2) - \gamma_0^{-1}\beta_2^2]J_m(z_2)H_m(z_2)\},\end{aligned}$$

(E18)

$$\begin{aligned}A_3(31) = &\{-[(P_2 - \beta_1^2) - x_1 x_2\beta_1^2]z_1' H_m'(z_1')J_m(z_1) + [(P_2 - \beta_2^2)\\ &- x_1 x_2\beta_2^2]z_2' H_m'(z_2')J_m(z_2) + S_{32}P_2 H_m(z_1')J_m(z_1)\\ &- S_{32}P_2 H_m(z_2')J_m(z_2)\},\end{aligned}$$

(E19)

$$\begin{aligned}A_3(41) = &\{+x_1 P_2 z_1' H_m'(z_1')J_m(z_1) - x_1 P_2 z_2' H_m'(z_2')J_m(z_2)\\ &+ S_{34}[(P_2 - \beta_1^2) - \gamma_0^{-1}\beta_1^2]H_m(z_1')J_m(z_1)\\ &- S_{34}[(P_2 - \beta_2^2) - \gamma_0^{-1}\beta_2^2]H_m(z_2')J_m(z_2)\},\end{aligned}$$

(E20)

$$\begin{aligned}A_3(12) = &\{+x_2 P_1 z_1 J_m'(z_1)H_m(z_1) - x_2 P_1 z_2 J_m'(z_2)H_m(z_2)\\ &+ S_{37}[(P_1 - \beta_1^2) - x_1 x_2\beta_1^2]J_m(z_1)H_m(z_1)\\ &- S_{37}[(P_1 - \beta_2^2) - x_1 x_2\beta_2^2]J_m(z_2)H_m(z_2)\},\end{aligned}$$

(E21)

$$\begin{aligned}A_3(22) = &\{+[(P_1 - \beta_1^2) - x_1 x_2\beta_1^2]z_1 J_m'(z_1)H_m(z_1) - [(P_1 - \beta_2^2)\\ &- x_1 x_2\beta_2^2]z_2 J_m'(z_2)H_m(z_2) - S_{38}[(P_1 - \beta_1^2)\\ &+ \gamma_0 x_1 x_2\beta_1^2]J_m(z_1)H_m(z_1) + S_{38}[(P_1 - \beta_2^2)\\ &+ \gamma_0 x_1 x_2\beta_2^2]J_m(z_2)H_m(z_2)\},\end{aligned}$$

(E22)

$$A_3(32) = \{-x_2 P_1 z_1' H_m'(z_1') J_m(z_1) + x_2 P_1 z_2' H_m'(z_2') J_m(z_2)$$
$$-S_{37}[(P_1 - \beta_1^2) - x_1 x_2 \beta_1^2] H_m(z_1') J_m(z_1)$$
$$+S_{37}[(P_1 - \beta_2^2) - x_1 x_2 \beta_2^2] H_m(z_2') J_m(z_2)\}, \quad \text{(E23)}$$

$$A_3(42) = \{-[(P_1 - \beta_1^2) - x_1 x_2 \beta_1^2] z_1' H_m'(z_1') J_m(z_1) + [(P_1 - \beta_2^2)$$
$$-x_1 x_2 \beta_2^2] z_2' H_m'(z_2') J_m(z_2) + S_{38}[(P_1 - \beta_1^2)$$
$$+\gamma_0 x_1 x_2 \beta_1^2] H_m(z_1') J_m(z_1) - S_{38}[(P_1 - \beta_2^2)$$
$$+\gamma_0 x_1 x_2 \beta_2^2] H_m(z_2') J_m(z_2)\}, \quad \text{(E24)}$$

$$A_3(13) = \{[(P_2 - \beta_1^2) - x_1 x_2 \beta_1^2] z_1 J_m'(z_1) H_m(z_1') - [(P_2 - \beta_2^2)$$
$$-x_1 x_2 \beta_2^2] z_2 J_m'(z_2) H_m(z_2') - S_{32} P_2 J_m(z_1) H_m(z_1')$$
$$+S_{32} P_2 J_m(z_2) H_m(z_2')\}, \quad \text{(E25)}$$

$$A_3(23) = \{-x_1 P_2 z_1 J_m'(z_1) H_m(z_1') + x_1 P_2 z_2 J_m'(z_2) H_m(z_2')$$
$$-S_{34}[(P_2 - \beta_1^2) - \gamma_0^{-1} \beta_1^2] J_m(z_1) H_m(z_1')$$
$$+S_{34}[(P_2 - \beta_2^2) - \gamma_0^{-1} \beta_2^2] J_m(z_2) H_m(z_2')\}, \quad \text{(E26)}$$

$$A_3(33) = \{-[(P_2 - \beta_1^2) - x_1 x_2 \beta_1^2] z_1' H_m'(z_1') J_m(z_1') + [(P_2 - \beta_2^2)$$
$$-x_1 x_2 \beta_2^2] z_2' H_m'(z_2') J_m(z_2') + S_{32} P_2 H_m(z_1') J_m(z_1')$$
$$-S_{32} P_2 H_m(z_2') J_m(z_2')\}, \quad \text{(E27)}$$

$$A_3(43) = \{+x_1 P_2 z_1' H_m'(z_1') J_m(z_1') - x_1 P_2 z_2' H_m'(z_2') J_m(z_2')$$
$$+S_{34}[(P_2 - \beta_1^2) - \gamma_0^{-1} \beta_1^2] H_m(z_1') J_m(z_1')$$
$$-S_{34}[(P_2 - \beta_2^2) - \gamma_0^{-1} \beta_2^2] H_m(z_2') J_m(z_2')\}, \quad \text{(E28)}$$

$$A_3(14) = \{+x_2 P_1 z_1 J_m'(z_1) H_m(z_1') - x_2 P_1 z_2 J_m'(z_2) H_m(z_2')$$
$$+S_{37}[(P_1 - \beta_1^2) - x_1 x_2 \beta_1^2] J_m(z_1) H_m(z_1')$$
$$-S_{37}[(P_1 - \beta_2^2) - x_1 x_2 \beta_2^2] J_m(z_2) H_m(z_2')\}, \quad \text{(E29)}$$

$$A_3(24) = \{+[(P_1 - \beta_1^2) - x_1 x_2 \beta_1^2] z_1 J_m'(z_1) H_m(z_1') - [(P_1 - \beta_2^2)$$
$$-x_1 x_2 \beta_2^2] z_2 J_m'(z_2) H_m(z_2') - S_{38}[(P_1 - \beta_1^2)$$
$$+\gamma_0 x_1 x_2 \beta_1^2] J_m(z_1) H_m(z_1') + S_{38}[(P_1 - \beta_2^2)$$
$$+\gamma_0 x_1 x_2 \beta_2^2] J_m(z_2) H_m(z_2')\}, \quad \text{(E30)}$$

$$A_3(34) = \{-x_2 P_1 z_1' H_m'(z_1') J_m(z_1') + x_2 P_1 z_2' H_m'(z_2') J_m(z_2')$$
$$-S_{37}[(P_1 - \beta_1^2) - x_1 x_2 \beta_1^2] H_m(z_1') J_m(z_1')$$
$$+S_{37}[(P_1 - \beta_2^2) - x_1 x_2 \beta_2^2] H_m(z_2') J_m(z_2')\}, \quad \text{(E31)}$$

$$A_3(44) = \{-[(P_1 - \beta_1^2) - x_1 x_2 \beta_1^2] z_1' H_m'(z_1') J_m(z_1') + [(P_1 - \beta_2^2)$$
$$-x_1 x_2 \beta_2^2] z_2' H_m'(z_2') J_m(z_2') + S_{38}[(P_1 - \beta_1^2)$$
$$+\gamma_0 x_1 x_2 \beta_1^2] H_m(z_1') J_m(z_1') - S_{38}[(P_1 - \beta_2^2)$$
$$+\gamma_0 x_1 x_2 \beta_2^2] H_m(z_2') J_m(z_2')\}, \quad \text{(E32)}$$

where $z_1 = \beta_1 R_1$, $z_2 = \beta_2 R_1$, $z_1' = \beta_1 R_2$, and $z_2' = \beta_2 R_2$. The prime on the Bessel functions stands for the derivative of the respective quantity with respect to the full argument. The matrix elements in Eq. (3.24) are defined as follows:

$$\Delta_3(11) = A_3(11), \quad \text{with } J_m' H_m \text{ replaced by } H_m' J_m, \quad \text{(E33)}$$

$$\Delta_3(21) = A_3(21), \quad \text{with } J_m' H_m \text{ replaced by } H_m' J_m, \quad \text{(E34)}$$

$$\Delta_3(31) = A_3(31), \quad \text{with } H_m' J_m \text{ replaced by } J_m' H_m, \quad \text{(E35)}$$

$$\Delta_3(41) = A_3(41), \quad \text{with } H_m' J_m \text{ replaced by } J_m' H_m, \quad \text{(E36)}$$

$$\Delta_3(12) = A_3(12), \quad \text{with } J_m' H_m \text{ replaced by } H_m' J_m, \quad \text{(E37)}$$

$$\Delta_3(22) = A_3(22), \quad \text{with } J_m' H_m \text{ replaced by } H_m' J_m, \quad \text{(E38)}$$

$$\Delta_3(32) = A_3(32), \quad \text{with } H_m' J_m \text{ replaced by } J_m' H_m, \quad \text{(E39)}$$

$$\Delta_3(42) = A_3(42), \quad \text{with } H_m' J_m \text{ replaced by } J_m' H_m, \quad \text{(E40)}$$

$$\Delta_3(13) = A_3(13), \quad \text{with } J_m' H_m \text{ replaced by } H_m' J_m, \quad \text{(E41)}$$

$$\Delta_3(23) = A_3(23), \quad \text{with } J_m' H_m \text{ replaced by } H_m' J_m, \quad \text{(E42)}$$

$$\Delta_3(33) = A_3(33), \quad \text{with } H_m' J_m \text{ replaced by } J_m' H_m, \quad \text{(E43)}$$

$$\Delta_3(43) = A_3(43), \quad \text{with } H_m' J_m \text{ replaced by } J_m' H_m, \quad \text{(E44)}$$

$$\Delta_3(14) = A_3(14), \quad \text{with } J_m' H_m \text{ replaced by } H_m' J_m, \quad \text{(E45)}$$

$$\Delta_3(24) = A_3(24), \quad \text{with } J_m' H_m \text{ replaced by } H_m' J_m, \quad \text{(E46)}$$

$$\Delta_3(34) = A_3(34), \quad \text{with } H_m' J_m \text{ replaced by } J_m' H_m, \quad \text{(E47)}$$

$$\Delta_3(44) = A_3(44), \quad \text{with } H_m' J_m \text{ replaced by } J_m' H_m. \quad \text{(E48)}$$

The matrix elements in Eq. (3.25) are defined as follows:

$$G_3^{-1}(11) = \frac{1}{S_{35}}\{+(P_1-\beta_1^2)[H_m(z_1)J_m(z_1')$$
$$-H_m(z_1')J_m(z_1)]J_m(z_1)J_m(z_2') - (P_1-\beta_2^2)$$
$$\times [H_m(z_2)J_m(z_2') - H_m(z_2')J_m(z_2)]J_m(z_1')J_m(z_2)\}$$
$$\times H_m(z_1')H_m(z_2'), \qquad (E49)$$

$$G_3^{-1}(21) = \frac{S_{33}}{S_{35}}\{+\beta_1^2[H_m(z_1)J_m(z_1')$$
$$-H_m(z_1')J_m(z_1)]J_m(z_1)J_m(z_2') - \beta_2^2[H_m(z_2)J_m(z_2')$$
$$-H_m(z_2')J_m(z_2)]J_m(z_1')J_m(z_2)\}H_m(z_1')H_m(z_2'),$$
$$(E50)$$

$$G_3^{-1}(31) = \frac{1}{S_{35}}\{-(P_1-\beta_1^2)[H_m(z_1)J_m(z_1') - H_m(z_1')J_m(z_1)]$$
$$+(P_1-\beta_2^2)[H_m(z_2)J_m(z_2') - H_m(z_2')J_m(z_2)]\}$$
$$\times J_m(z_1)J_m(z_2)H_m(z_1')H_m(z_2'), \qquad (E51)$$

$$G_3^{-1}(41) = \frac{S_{33}}{S_{35}}\{-\beta_1^2[H_m(z_1)J_m(z_1') - H_m(z_1')J_m(z_1)]$$
$$+\beta_2^2[H_m(z_2)J_m(z_2') - H_m(z_2')J_m(z_2)]\}$$
$$\times J_m(z_1)J_m(z_2)H_m(z_1')H_m(z_2'), \qquad (E52)$$

$$G_3^{-1}(12) = \frac{S_{36}}{S_{31}}\{-\beta_1^2[H_m(z_1)J_m(z_1')$$
$$-H_m(z_1')J_m(z_1)]J_m(z_1)J_m(z_2') + \beta_2^2[H_m(z_2)J_m(z_2')$$
$$-H_m(z_2')J_m(z_2)]J_m(z_1')J_m(z_2)\}H_m(z_1')H_m(z_2'),$$
$$(E53)$$

$$G_3^{-1}(22) = \frac{1}{S_{31}}\{+(P_1-\beta_1^2)[H_m(z_1)J_m(z_1')$$
$$-H_m(z_1')J_m(z_1)]J_m(z_1)J_m(z_2') - (P_2-\beta_2^2)$$
$$\times [H_m(z_2)J_m(z_2') - H_m(z_2')J_m(z_2)]J_m(z_1')J_m(z_2)\}$$
$$\times H_m(z_1')H_m(z_2'), \qquad (E54)$$

$$G_3^{-1}(32) = \frac{S_{36}}{S_{31}}\{+\beta_1^2[H_m(z_1)J_m(z_1') - H_m(z_1')J_m(z_1)]$$
$$-\beta_2^2[H_m(z_2)J_m(z_2') - H_m(z_2')J_m(z_2)]\}$$
$$\times J_m(z_1)J_m(z_2)H_m(z_1')H_m(z_2'), \qquad (E55)$$

$$G_3^{-1}(42) = \frac{1}{S_{31}}\{-(P_2-\beta_1^2)[H_m(z_1)J_m(z_1') - H_m(z_1')J_m(z_1)]$$
$$+(P_2-\beta_2^2)[H_m(z_2)J_m(z_2') - H_m(z_2')J_m(z_2)]\}$$
$$\times J_m(z_1)J_m(z_2)H_m(z_1')H_m(z_2'), \qquad (E56)$$

$$G_3^{-1}(13) = \frac{1}{S_{35}}\{-(P_1-\beta_1^2)[H_m(z_1)J_m(z_1') - H_m(z_1')J_m(z_1)]$$
$$+(P_1-\beta_2^2)[H_m(z_2)J_m(z_2') - H_m(z_2')J_m(z_2)]\}$$
$$\times J_m(z_1)J_m(z_2)H_m(z_1')H_m(z_2'), \qquad (E57)$$

$$G_3^{-1}(23) = \frac{S_{33}}{S_{35}}\{-\beta_1^2[H_m(z_1)J_m(z_1') - H_m(z_1')J_m(z_1)]$$
$$+\beta_2^2[H_m(z_2)J_m(z_2') - H_m(z_2')J_m(z_2)]\}$$
$$\times J_m(z_1)J_m(z_2)H_m(z_1')H_m(z_2'), \qquad (E58)$$

$$G_3^{-1}(33) = \frac{1}{S_{35}}\{+(P_1-\beta_1^2)[H_m(z_1)J_m(z_1')$$
$$-H_m(z_1')J_m(z_1)]H_m(z_1')H_m(z_2) - (P_1-\beta_2^2)$$
$$\times [H_m(z_2)J_m(z_2') - H_m(z_2')J_m(z_2)]H_m(z_1)H_m(z_2')\}$$
$$\times J_m(z_1)J_m(z_2), \qquad (E59)$$

$$G_3^{-1}(43) = \frac{S_{33}}{S_{35}}\{+\beta_1^2[H_m(z_1)J_m(z_1')$$
$$-H_m(z_1')J_m(z_1)]H_m(z_1')H_m(z_2) - \beta_2^2[H_m(z_2)J_m(z_2')$$
$$-H_m(z_2')J_m(z_2)]H_m(z_1)H_m(z_2')\}J_m(z_1)J_m(z_2),$$
$$(E60)$$

$$G_3^{-1}(14) = \frac{S_{36}}{S_{31}}\{-\beta_1^2[H_m(z_1)J_m(z_1') - H_m(z_1')J_m(z_1)]$$
$$+\beta_2^2[H_m(z_2)J_m(z_2') - H_m(z_2')J_m(z_2)]\}$$
$$\times J_m(z_1)J_m(z_2)H_m(z_1')H_m(z_2'), \qquad (E61)$$

$$G_3^{-1}(24) = \frac{1}{S_{31}}\{-(P_2-\beta_1^2)[H_m(z_1)J_m(z_1') - H_m(z_1')J_m(z_1)]$$
$$+(P_2-\beta_2^2)[H_m(z_2)J_m(z_2') - H_m(z_2')J_m(z_2)]\}$$
$$\times J_m(z_1)J_m(z_2)H_m(z_1')H_m(z_2'), \qquad (E62)$$

$$G_3^{-1}(34) = \frac{S_{36}}{S_{31}}\{-\beta_1^2[H_m(z_1)J_m(z_1')$$
$$-H_m(z_1')J_m(z_1)]H_m(z_1')H_m(z_2) + \beta_2^2[H_m(z_2)J_m(z_2')$$
$$-H_m(z_2')J_m(z_2)]H_m(z_1)H_m(z_2')\}J_m(z_1)J_m(z_2),$$
$$(E63)$$

$$G_3^{-1}(44) = \frac{1}{S_{31}}\{+(P_2-\beta_1^2)[H_m(z_1)J_m(z_1')$$
$$-H_m(z_1')J_m(z_1)]H_m(z_1')H_m(z_2) - (P_2-\beta_2^2)$$
$$\times [H_m(z_2)J_m(z_2') - H_m(z_2')J_m(z_2)]H_m(z_1)H_m(z_2')\}$$
$$\times J_m(z_1)J_m(z_2). \qquad (E64)$$

Finally, the matrix elements in Eq. (3.28) are given by

$$h_3(11) = S_{31}\left\{ -S_{32}(\beta_1^2 - \beta_2^2) - (P_1 - \beta_1^2) \right.$$
$$\times z_2\frac{H'_m(z_2)J_m(z_2') - H_m(z_2')J'_m(z_2)}{H_m(z_2)J_m(z_2') - H_m(z_2')J_m(z_2)} + (P_1 - \beta_2^2)$$
$$\left. \times z_1\frac{H'_m(z_1)J_m(z_1') - H_m(z_1')J'_m(z_1)}{H_m(z_1)J_m(z_1') - H_m(z_1')J_m(z_1)} \right\}, \quad (E65)$$

$$h_3(21) = S_{31}\left\{ -S_{34}(\beta_1^2 - \beta_2^2) \right.$$
$$- \beta_1^2 x_1 z_2\frac{H'_m(z_2)J_m(z_2') - H_m(z_2')J'_m(z_2)}{H_m(z_2)J_m(z_2') - H_m(z_2')J_m(z_2)}$$
$$\left. + \beta_2^2 x_1 z_1\frac{H'_m(z_1)J_m(z_1') - H_m(z_1')J'_m(z_1)}{H_m(z_1)J_m(z_1') - H_m(z_1')J_m(z_1)} \right\}, \quad (E66)$$

$$h_3(31) = S_{31}\left\{ +(P_1 - \beta_1^2)z_2'\frac{H'_m(z_2')J_m(z_2) - H_m(z_2')J'_m(z_2)}{H_m(z_2)J_m(z_2') - H_m(z_2')J_m(z_2)} \right.$$
$$\left. - (P_1 - \beta_2^2)z_1'\frac{H'_m(z_1')J_m(z_1) - H_m(z_1')J'_m(z_1)}{H_m(z_1)J_m(z_1') - H_m(z_1')J_m(z_1)} \right\}, \quad (E67)$$

$$h_3(41) = S_{31}\left\{ +\beta_1^2 x_1 z_2'\frac{H'_m(z_2')J_m(z_2) - H_m(z_2')J'_m(z_2)}{H_m(z_2)J_m(z_2') - H_m(z_2')J_m(z_2)} \right.$$
$$\left. - \beta_2^2 x_1 z_1'\frac{H'_m(z_1')J_m(z_1) - H_m(z_1')J'_m(z_1)}{H_m(z_1)J_m(z_1') - H_m(z_1')J_m(z_1)} \right\}, \quad (E68)$$

$$h_3(12) = S_{35}\left\{ +S_{37}(\beta_1^2 - \beta_2^2) \right.$$
$$+ \beta_1^2 x_2 z_2\frac{H'_m(z_2)J_m(z_2') - H_m(z_2')J'_m(z_2)}{H_m(z_2)J_m(z_2') - H_m(z_2')J_m(z_2)}$$
$$\left. - \beta_2^2 x_2 z_1\frac{H'_m(z_1)J_m(z_1') - H_m(z_1')J'_m(z_1)}{H_m(z_1)J_m(z_1') - H_m(z_1')J_m(z_1)} \right\}, \quad (E69)$$

$$h_3(22) = S_{35}\left\{ -S_{38}(\beta_1^2 - \beta_2^2) - (P_2 - \beta_1^2) \right.$$
$$\times z_2\frac{H'_m(z_2)J_m(z_2') - H_m(z_2')J'_m(z_2)}{H_m(z_2)J_m(z_2') - H_m(z_2')J_m(z_2)} + (P_2 - \beta_2^2)$$
$$\left. \times z_1\frac{H'_m(z_1)J_m(z_1') - H_m(z_1')J'_m(z_1)}{H_m(z_1)J_m(z_1') - H_m(z_1')J_m(z_1)} \right\}, \quad (E70)$$

$$h_3(32) = S_{35}\left\{ -\beta_1^2 x_2 z_2'\frac{H'_m(z_2')J_m(z_2) - H_m(z_2')J'_m(z_2)}{H_m(z_2)J_m(z_2') - H_m(z_2')J_m(z_2)} \right.$$
$$\left. + \beta_2^2 x_2 z_1'\frac{H'_m(z_1')J_m(z_1) - H_m(z_1')J'_1(z_1')}{H_m(z_1)J_m(z_1') - H_m(z_1')J_m(z_1)} \right\}, \quad (E71)$$

$$h_3(42) = S_{35}\left\{ +(P_2 - \beta_1^2)z_2'\frac{H'_m(z_2')J_m(z_2) - H_m(z_2')J'_m(z_2)}{H_m(z_2)J_m(z_2') - H_m(z_2')J_m(z_2)} \right.$$
$$\left. - (P_2 - \beta_2^2)z_1'\frac{H'_m(z_1')J_m(z_1) - H_m(z_1')J'_m(z_1)}{H_m(z_1)J_m(z_1') - H_m(z_1')J_m(z_1)} \right\}, \quad (E72)$$

$$h_3(13) = S_{31}\left\{ +(P_1 - \beta_1^2)z_2\frac{H'_m(z_2)J_m(z_2) - H_m(z_2)J'_m(z_2)}{H_m(z_2)J_m(z_2') - H_m(z_2')J_m(z_2)} \right.$$
$$\left. - (P_1 - \beta_2^2)z_1\frac{H'_m(z_1)J_m(z_1) - H_m(z_1)J'_m(z_1)}{H_m(z_1)J_m(z_1') - H_m(z_1')J_m(z_1)} \right\}, \quad (E73)$$

$$h_3(23) = S_{31}\left\{ +\beta_1^2 x_1 z_2\frac{H'_m(z_2)J_m(z_2) - H_m(z_2)J'_m(z_2)}{H_m(z_2)J_m(z_2') - H_m(z_2')J_m(z_2)} \right.$$
$$\left. - \beta_2^2 x_1 z_1\frac{H'_m(z_1)J_m(z_1) - H_m(z_1)J'_m(z_1)}{H_m(z_1)J_m(z_1') - H_m(z_1')J_m(z_1)} \right\}, \quad (E74)$$

$$h_3(33) = S_{31}\left\{ +S_{32}(\beta_1^2 - \beta_2^2) - (P_1 - \beta_1^2) \right.$$
$$\times z_2'\frac{H'_m(z_2')J_m(z_2) - H_m(z_2)J'_m(z_2')}{H_m(z_2)J_m(z_2') - H_m(z_2')J_m(z_2)} + (P_1 - \beta_2^2)$$
$$\left. \times z_1'\frac{H'_m(z_1')J_m(z_1) - H_m(z_1)J'_m(z_1')}{H_m(z_1)J_m(z_1') - H_m(z_1')J_m(z_1)} \right\}, \quad (E75)$$

$$h_3(43) = S_{31}\left\{ +S_{34}(\beta_1^2 - \beta_2^2) \right.$$
$$- \beta_1^2 x_1 z_2'\frac{H'_m(z_2')J_m(z_2) - H_m(z_2)J'_m(z_2')}{H_m(z_2)J_m(z_2') - H_m(z_2')J_m(z_2)}$$
$$\left. + \beta_2^2 x_1 z_1'\frac{H'_m(z_1')J_m(z_1) - H_m(z_1)J'_m(z_1')}{H_m(z_1)J_m(z_1') - H_m(z_1')J_m(z_1)} \right\}, \quad (E76)$$

$$h_3(14) = S_{35}\left\{ -\beta_1^2 x_2 z_2\frac{H'_m(z_2)J_m(z_2) - H_m(z_2)J'_m(z_2)}{H_m(z_2)J_m(z_2') - H_m(z_2')J_m(z_2)} \right.$$
$$\left. + \beta_2^2 x_2 z_1\frac{H'_m(z_1)J_m(z_1) - H_m(z_1)J'_m(z_1)}{H_m(z_1)J_m(z_1') - H_m(z_1')J_m(z_1)} \right\}, \quad (E77)$$

$$h_3(24) = S_{35}\left\{ +(P_2 - \beta_1^2)z_2\frac{H'_m(z_2)J_m(z_2) - H_m(z_2)J'_m(z_2)}{H_m(z_2)J_m(z_2') - H_m(z_2')J_m(z_2)} \right.$$
$$\left. - (P_2 - \beta_2^2)z_1\frac{H'_m(z_1)J_m(z_1) - H_m(z_1)J'_m(z_1)}{H_m(z_1)J_m(z_1') - H_m(z_1')J_m(z_1)} \right\}, \quad (E78)$$

$$h_3(34) = S_{35}\Bigg\{ -S_{37}(\beta_1^2 - \beta_2^2)$$

$$+ \beta_1^2 x_2 z_2' \frac{H_m'(z_2')J_m(z_2) - H_m(z_2)J_m'(z_2')}{H_m(z_2)J_m(z_2') - H_m(z_2')J_m(z_2)}$$

$$- \beta_2^2 x_2 z_1' \frac{H_m'(z_1')J_m(z_1) - H_m(z_1)J_m'(z_1')}{H_m(z_1)J_m(z_1') - H_m(z_1')J_m(z_1)} \Bigg\},$$

$$\text{(E79)}$$

$$h_3(44) = S_{35}\Bigg\{ +S_{38}(\beta_1^2 - \beta_2^2) - (P_2 - \beta_1^2)$$

$$\times z_2' \frac{H_m'(z_2')J_m(z_2) - H_m(z_2)J_m'(z_2')}{H_m(z_2)J_m(z_2') - H_m(z_2')J_m(z_2)} + (P_2 - \beta_2^2)$$

$$\times z_1' \frac{H_m'(z_1')J_m(z_1) - H_m(z_1)J_m'(z_1')}{H_m(z_1)J_m(z_1') - H_m(z_1')J_m(z_1)} \Bigg\}.$$

$$\text{(E80)}$$

[1] For a recent extensive review of the electronic, optical, and transport properties of the systems of reduced dimensionality, such as quantum wells, wires, dots, and modulated 2D systems, see M. S. Kushwaha, Surf. Sci. Rep. **41**, 1 (2001).

[2] V. Fock, Phys. Z. **47**, 446 (1928); C. G. Darwin, Proc. Cambridge Philos. Soc. **27**, 86 (1930).

[3] F. Bloch, Phys. Z. **52**, 555 (1928).

[4] L. D. Landau, Phys. Z. **64**, 269 (1930).

[5] L. W. Shubnikov and W. J. de Haas, Commun. Kamerlingh Onnes Lab. Univ. Leiden, Suppl. **207**, 210 (1930).

[6] W. J. de Haas and P. M. van Alphen, Commun. Kamerlingh Onnes Lab. Univ. Leiden, Suppl. **212**, 215 (1930).

[7] R. B. Dingle, Proc. R. Soc. London, Ser. A **211**, 517 (1952); M. Ya. Azbel' and E. A. Kaner, Sov. Phys. JETP **3**, 772 (1956).

[8] D. Hofstadter, Phys. Rev. B **14**, 2239 (1976); D. Langbein, Phys. Rev. **180**, 633 (1969); P. G. Harper, Proc. Phys. Soc., London, Sect. A **68**, 879 (1955).

[9] K. v. Klitzing, G. Dorda, and M. Pepper, Phys. Rev. Lett. **45**, 494 (1980); D. C. Tsui, H. L. Stormer, and A. C. Gossard, Phys. Rev. Lett. **48**, 1559 (1982).

[10] P. S. Drouvelis, P. Schmelcher, and F. K. Diakonos, Phys. Rev. B **69**, 155312 (2004).

[11] C. L. Foden, M. L. Leadbeater, and M. Pepper, Phys. Rev. B **52**, R8646 (1995).

[12] G. D. Banyard, C. R. Bennett, and M. Babiker, Opt. Commun. **207**, 195 (2002).

[13] L. Dobrzynski, Surf. Sci. Rep. **6**, 119 (1986); Surf. Sci. **300**, 1008 (1994).

[14] L. Dobrzynski and H. Puszkarski, J. Phys.: Condens. Matter **1**, 1239 (1989).

[15] M. S. Kushwaha and B. Djafari-Rouhani, Phys. Rev. B **43**, 9021 (1991); Surf. Sci. **244**, 336 (1991); **268**, 457 (1992).

[16] B. Djafari-Rouhani and L. Dobrzynski, J. Phys.: Condens. Matter **5**, 139 (1993).

[17] M. S. Kushwaha and B. Djafari-Rouhani, Phys. Rev. B **57**, 13020 (1998).

[18] M. S. Kushwaha and B. Djafari-Rouhani, Ann. Phys. (N.Y.) **265**, 1 (1998).

[19] M. S. Kushwaha and B. Djafari-Rouhani, Phys. Rev. B **67**, 245320 (2003).

[20] H. Khosravi, D. R. Tilley, and R. Loudon, J. Opt. Soc. Am. A **8**, 112 (1991); R. Rupin, in *Electromagnetic Surface Modes*, edited by A. D. Boardman (Wiley, New York, 1982), p. 389; G. C. Aers, A. D. Boardman, and B. V. Paranjape, J. Phys. F: Met. Phys. **10**, 53 (1980).

[21] J. Kong, L. Kouwenhoven, and C. Dekker, Phys. World **17**(7), 33 (2004).

[22] P. M. Morse and H. Feshbach, *Methods of Theoretical Physics* (McGraw-Hill, New York, 1953), Vol. 2.

[23] M. Abramowitz and I. A. Stegun, *Handbook of Mathematical Functions* (Dover, New York, 1972).

[24] R. F. Wallis, in *Electromagnetic Surface Modes*, edited by A. D. Boardman (Wiley, New York, 1982), p. 575.

[25] M. S. Kushwaha and P. Halevi, Phys. Rev. B **35**, 3879 (1987).